Ionogram Scaling for Vertical, Oblique, And Backscatter Sounders

A review of challenges and opportunities

RAFAL SIENICKI, DANIELLE J. EDWARDS, MANUEL A. CERVERA, AND PHILIP H. W. LEONG

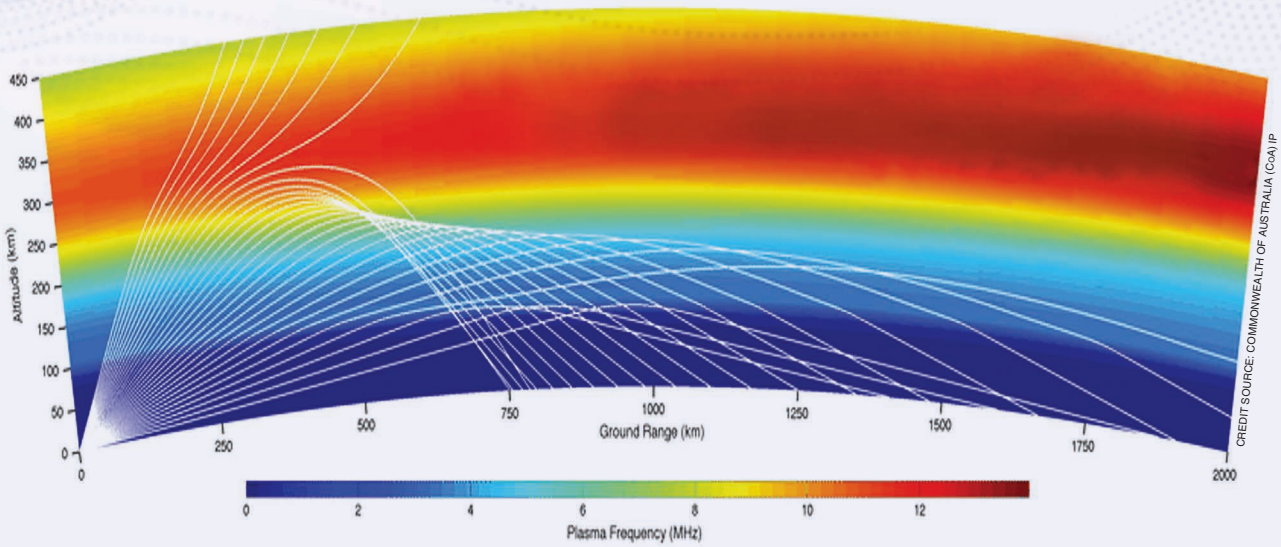

The process of feature identification in ionogram images and subsequent derivation of ionospheric parameters, known as *ionogram scaling*, enables the characterization of the ionospheric propagation conditions of radio waves in the high-frequency (HF) band. Manual ionogram scaling is a time-intensive and laborious activity; hence, numerous techniques have been developed by many researchers to automate this task.

This article presents a review of the various automatic scaling approaches applicable to vertical, oblique, and backscatter ionograms. In addition, we provide a set of recommendations to guide and stimulate further research in this field.

Digital Object Identifier 10.1109/MGRS.2025.3602369

INTRODUCTION

The ionosphere is a region of Earth's atmosphere that contains free electrons and is able to refract HF (3–30-MHz) radio waves. This can be exploited to enable long-range and beyond-line-of-sight capabilities such as remote sensing, communications, and surveillance. The ionosphere is a highly dynamic medium that varies temporally and spatially over many different scales; hence, characterization of the ionosphere is crucial for the effective operation of any HF system.

Ionospheric sounder equipment is used to measure and quantify the properties of the ionosphere by the transmission and reception of HF radio waves. Vertical incidence sounders (VISs) and oblique incidence sounders (OISs) are typically used for this purpose. A VIS measures the ionospheric properties directly above (the receiver

and transmitter are colocated), while an OIS measures the ionosphere at the midpoint between a transmitter and a receiver several hundreds or thousands of kilometers away. VIS, and to a lesser extent, OIS systems are widely deployed around the globe for the purpose of global ionospheric characterization [1].

The backscatter sounder (BSS) is another type of sounder system. These systems receive the ionospherically propagated radio waves from the transmitter via backscatter from the ground or sea. Consequently, BSS systems require a greater transmit power and are more complex than VIS and OIS systems. They are useful for the support of a long-range surveillance radar, such as over-the-horizon radar (OTHR), due to their similar two-way propagation paths [2].

The return signal strength when displayed as a function of group range[1] versus radio wave frequency is known as an *ionogram*. These ionograms are evaluated to identify critical features and parameters that subsequently can be used to infer the properties of the ionosphere and the ionospheric propagation conditions. This process is called ionogram scaling.[2] Traditionally, ionogram scaling has been performed by ionosphere subject matter experts (SMEs); however, manual scaling is a time-intensive and laborious activity, and hence, numerous automatic scaling techniques have been investigated and developed over the last few decades. The vast majority of automated scaling algorithms have been applied to VIS ionograms, and to a lesser extent, OIS ionograms, with limited attention to BSS ionograms. Automated scaling tools such as polynomial analysis (POLAN) [4], Automatic Real Time Ionogram Scaler with True Height (ARTIST) [5], Autoscala [6], and DST Ionogram Image Processing (DST-IIP) [7] have been demonstrated to reliably extract critical features in VIS ionograms. These tools are widely cited and are recognized as authoritative tools in the ionospheric research community. OISs are not as widely used as VISs. Consequently, there is a lack of OIS scaling tools that match the pedigree of the aforementioned VIS scaling tools; however, details of several algorithms have been published [7], [8], [9], [10].

The scaling of BSS ionograms is more challenging and the least mature. The integration of returns from multiple propagation modes and antenna sidelobes, the variable ground backscatter, and the reduced number of nonambiguous visually discernible image features increases the scaling complexity. Consequently, very few publications exist that detail methods and techniques for automated backscatter ionogram scaling.

This article presents a literature review of the various automatic scaling approaches applicable to vertical, oblique, and backscatter ionograms. To the best of our knowledge, this is the first comparative review of scaling approaches across all sounder types. While some VIS scaling investigations (e.g., see Lynn [11], Heitmann and Gardiner-Garden [7], and Xiao et al. [12]) include a summary of relevant techniques and methods, a dedicated comparative review across all sounder types has not been published.

MOTIVATION

Characterization of the ionosphere is a critical requirement for the operation of systems that use the ionosphere to provide a beyond-line-of-sight capability, such as communication, surveillance, or remote sensing. Inference of ionospheric propagation properties at the transmission reflection point is important for frequency management, calibration, and performance optimization of operational HF systems [2]. The structure of the ionosphere is highly nonstationary and varies according to diurnal, seasonal, and solar cycle variations as well as space weather-induced phenomena, and hence, ionospheric measurements are critical for accurate characterization of the ionosphere [2].

An ionogram records the return signal strength of sounder transmission signals propagated via the ionosphere. The return signal strength is typically represented as a 2D image, with frequency on the x axis and group range on the y axis. Usually, VIS ionograms use half the group range, referred to as virtual height,[3] on the y axis. Samples of ionogram images pertaining to vertical, oblique, and BSSs are shown later in the "Oblique Incidence Sounder" section and "Backscatter Sounder" section. Critical scaling features are labeled in these figures and indicate those features that are ideally identified by an automated scaling algorithm.

Ionogram scaling features are visually discernible as a series of curved connected trace segments representing a pattern of signal strength variation that is governed by the ionospheric propagation conditions. Each type of sounder produces unique trace segment patterns (features). Visual discernment of the critical features in ionograms is complicated by noise, interference, sounder equipment failures, returns from "unusual" ionospheric layers (e.g., sporadic E layers, described in the "Vertical Incidence Sounder Ionogram Features" section), and ionospheric disturbances. The effects of these phenomena can be observed on an ionogram as distortion, smearing, blurring, and masking of important ionogram features.

Parameterization of the ionogram image enables the tuning of electron density model parameters to produce a representative electron density profile based on the collected ionospheric measurements [13]. The characterization of the electron density distribution profile is a highly complex undertaking due to the nonstationarity, inhomogeneity, and

[1]Time-of-flight of the radio wave multiplied by the speed of light in vacuo.
[2]In this article, the term "scaling" is used in reference to all ionograms recorded by the three sounder types. We acknowledge that the term does not have the same meaning for VIS/OIS and BSS ionogram categories. In the former case, scaling refers to ionogram feature identification and parameterization of ionospheric properties [3], e.g., critical frequency, minimum virtual height. This is the conventional interpretation of the term in the ionospheric research community. In the latter case, the term refers to a more limited operation. Here, scaling refers to the identification of features from which information regarding the propagation modes may be inferred, without any subsequent ionospheric parameterization.

[3]The radio waves are retarded by the ionosphere, and so the measured, or virtual, height is greater than the true height of reflection.

scattering properties of the ionosphere. However, the electron density vertical profile can be estimated if certain assumptions are applied. The quasi-parabolic segments (QPS) model [14], [15] is one example. In this model, the electron density profile is defined by a set of quasi-parabolic functions that parameterize the main refracting layers of the ionosphere (viz., the E, F1, and F2 layers). The ionogram scaling parameters are used to define the coefficients of the quasi-parabolic functions pertaining to the E, F1, and F2 ionospheric layers.

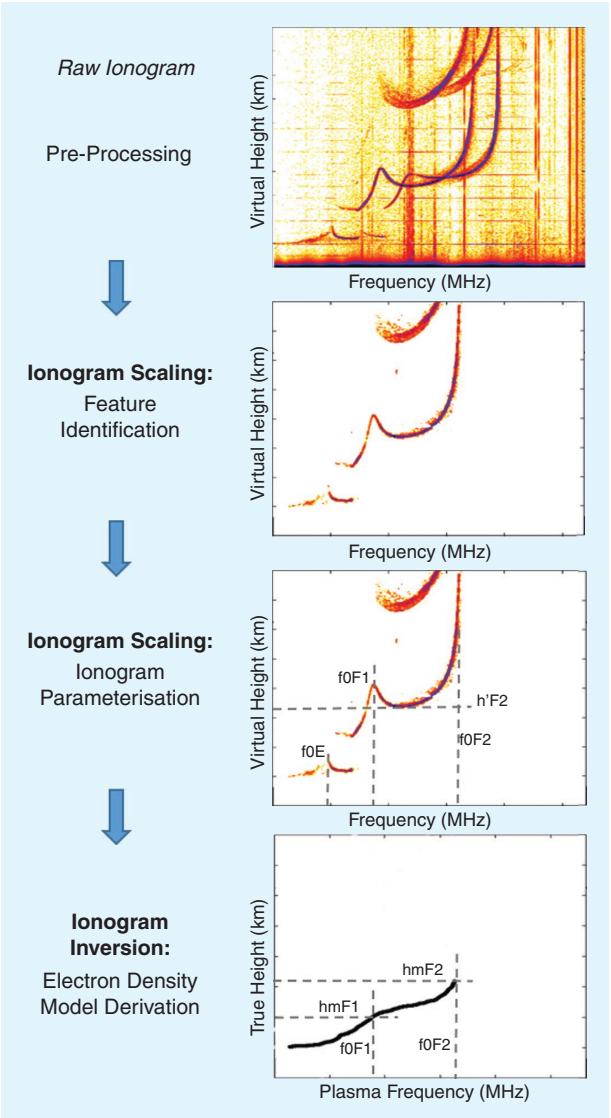

FIGURE 1. The workflow for VIS ionogram scaling. A sounder is used to record the return signal strength as a function of frequency. These measurements are formatted into an image known as an *ionogram*. Analysis of return signal strength intensity variation and shape (profile) of ionogram traces is used to identify key ionogram features that can subsequently be used to derive ionospheric parameters. This process is known as *ionogram scaling*. These parameters can be used to derive an estimate of the overhead electron density profile. This process is known as *ionogram inversion*. (Source: Generated by DST Group and CoA owned.)

The task of ionogram scaling is recognized as both an art and a science [16]. While accurate interpretation of ionogram features requires a deep understanding of the ionospheric physics and HF radio-wave propagation, the identification of features and interpolation and extrapolation of traces often requires a judgment call by an expert. It is therefore not uncommon to obtain variations in outputs even when the scaling is executed by a group of ionospheric SMEs. This is particularly true for the analysis of ionograms captured in disturbed ionospheric conditions. The subjective aspect of ionogram scaling is exacerbated for ionograms recorded by a BSS. Moreover, it is possible for no viable scaling solutions to be available for ionograms recorded during disturbed or anomalous ionospheric conditions and/or contaminated with a high level of noise and interference.

OVERVIEW AND SCOPE

Research on approaches and techniques for automatic ionogram scaling started in the 1960s [17], [18], [19], and numerous toolsets have been developed to perform this function. This article details a comprehensive review of key features, image artifacts, and attributes of VIS, OIS, and BSS ionograms and relevant scaling techniques and evaluation metrics.

The "Ionogram Scaling Workflow" section introduces the ionogram scaling workflow to provide context for the importance of ionogram feature identification and parameterization. The "Vertical Incidence Sounders," "Oblique Incidence Sounder," and "Backscatter Sounder" sections review ionogram features and automated scaling techniques for each sounder type. To the best of our knowledge, this is the first comparative review of scaling approaches across all types of ionospheric sounder systems. The "Ionogram Scaling Metrics" section reviews the metrics applied for the evaluation of ionogram scaling performance. The "Effects of Space Weather on Ionogram Feature Characteristics" section examines the influence of space weather, ionospheric disturbances, and sounder failures on ionogram feature characteristics and corresponding scaling challenges.

Over the last decade, there has been an increase in the number of publications covering machine learning (ML)-based investigations for application to automatic ionogram scaling. To this end, the "Review of Deep Learning Ionogram Scaling Investigations" section reviews and compares the merits of ML approaches for this use case. The "Discussion" section concludes this article with a set of findings and recommendations to guide and stimulate further research in this field.

A brief overview of the physics of the ionosphere, space weather, and sounder system design and configuration is included in this article to provide context for ionogram feature interpretation. This material will be beneficial to readers who do not have an ionospheric physics background.

In this review, we focus solely on ionograms recorded by bottom-side ionospheric soundings. Top-side, transionospheric, and reverse transionospheric sounding systems are not considered [20].

IONOGRAM SCALING WORKFLOW

The ultimate goal of ionogram scaling is to provide an estimate of the ionospheric properties and propagation conditions derived from sounder measurements. The ionogram scaling process involves a sequence of steps that are undertaken to enable inference of an electron density distribution model based on an input ionogram. The workflow for an end-to-end ionogram scaling process can be described as follows:

1) preprocessing[4] an ionogram image to reduce the effects of background noise (denoising) and interference
2) identification, separation, and extraction of dominant traces and features
3) derivation of critical ionospheric parameters from the extracted traces
4) derivation of the electron density vertical profile, a process referred to as ionogram inversion [26].

A visual depiction of the workflow for ionogram scaling and inversion is presented in Figure 1. The focus of this article is on the feature identification and ionogram parameterization steps of the ionogram scaling workflow.

VERTICAL INCIDENCE SOUNDERS

The VIS, also known as an *ionosonde*, is an HF radar that measures the vertical structure of the ionosphere directly above the instrument. The VIS sweeps up in frequency through the HF band and measures the time delay of the returns from the ionosphere. The height from which each frequency is reflected provides information about the different ionospheric layers. Figure 2 shows the configuration of a VIS system for vertical probing of the ionosphere.

Early VIS instruments measured the travel time of the ionospherically propagated radio waves to obtain the virtual height of reflection. With the addition of digital receiver technology, modern instruments. such as the Lowell Digisonde [1], also evaluate the angle of arrival, polarization, and Doppler shift of the reflected signals. This provides additional information to aid in the ionogram scaling.

The VIS is more commonly used than the OIS or BSS as it requires only a single site, operates at a lower power than is required for a BSS, gives a direct measure of the ionospheric critical frequency, and the exact location of the ionosphere that is being probed is more precisely known. Global networks of VIS systems have been established over time with large long-term datasets publicly available online. The most widely used network and dataset is provided by the Global Ionosphere Radio Observatory (GIRO) [1]. Some examples of other networks and datasets include those hosted by the Australian Space Weather Forecasting Center [27] and the SEALION network operated by the National Institute of Information and Communications Technology (NICT), Japan [28]. For a historical overview of early VIS development, the interested reader is referred to Gladden et. al [29].

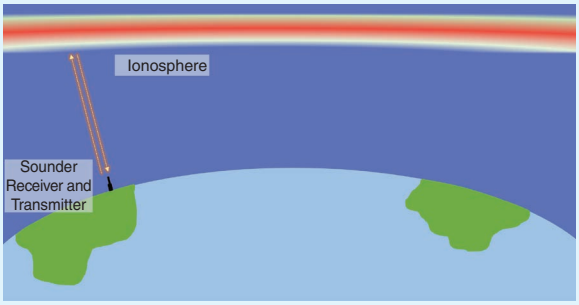

FIGURE 2. A simplified diagram (not to scale) showing VIS operation. Sounder signal reflections from the overhead ionosphere can be used to infer the electron density profile.

VERTICAL INCIDENCE SOUNDER IONOGRAM FEATURES

A typical VIS ionogram is presented in Figure 3(a). The reflection of the sounder transmission signal as a function of frequency and group range is shown as a curved trace with a series of peaks, known as *cusps*, culminating with the terminal trace segment extending asymptotically to the top of the image [20]. The second hop trace [labeled as "second hop F2" in Figure 3(a)] is due to the reflection of the radio waves from the ionosphere to the ground back to the ionosphere and then to the receiver. It is not important for deriving ionospheric parameters and will not be discussed further.

Two traces are noted, offset in frequency and group range. This is due to the birefringent[5] property of the ionosphere, causing the radio wave to split into left- and right-handed elliptically polarized waves. The trace that asymptotes at the lower frequency is the ordinary (O) mode, and the other is the extraordinary (X) mode. The O mode is so named as, for vertical propagation, the radio wave is reflected at an altitude where the plasma frequency[6] of the ionosphere is equal to the radio wave frequency. In the majority of ionograms captured during daytime, it is common to observe up to three cusps due to reflections from three distinct layers of the ionosphere: the E, F1, and F2 layers. The interpretation of frequency and height parameters of ionogram features corresponding to these layers enables the definition of an electron density profile.

The rapidly increasing retardation of the radio waves with frequency immediately prior to the penetration of the ionosphere results in the corresponding feature being the most visually prominent [left vertical asymptote line labeled in Figure 3(a)]. The frequency at which

[4]Preprocessing is an important prerequisite step in the scaling workflow. Techniques such as signal processing (e.g., Fourier transform [21]), image processing (e.g., morphological operators [9] and edge detection [22]), filtering (e.g., size contrast filter [23], grayscaling [24], and thresholding [24], [25]) have been investigated for ionogram preprocessing.

[5]Earth's magnetic field causes the refractive index of the ionosphere to have different values depending upon the orientation of the radio wave polarization.

[6]Plasma frequency f_N is related to electron density N_e by the equation $f_N = (N_e e^2/\epsilon_0 m)^{1/2}$ [20], where e and m are the charge and mass of an electron, respectively, and ϵ_0 is the permittivity of free space.

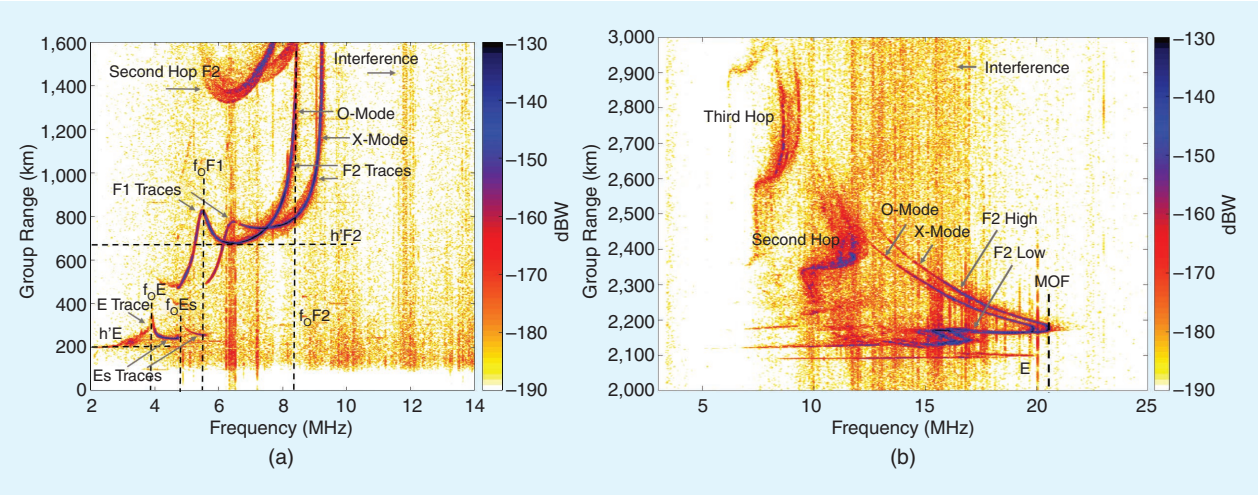

FIGURE 3. Sample VIS and OIS ionograms highlighting key ionogram scaling features. Returns from higher-order hops and interference artifacts are also labeled. (a) VIS ionogram with key scaling features labeled. (b) OIS ionogram with key features labeled. (Source: Generated by DST Group and CoA owned.)

this feature occurs is known as f_oF2 and is the critical frequency of the ionosphere. Vertically propagating O-mode radio waves above this frequency penetrate the ionosphere. The cusps to the left of the f_oF2 feature correspond to the critical frequencies of the E and F1 layers. The frequencies at which these features occur are known as f_oE and f_oF1, respectively.

The virtual height (half of the group range) for the E, F1, and F2 features can be read from the y axis. Minimum virtual heights corresponding to E, F1, and F2 layers are labeled as h'E, h'F1, and h'F2, respectively, in Figure 3(a). Note that the virtual height of reflection is greater than the true height due to the retardation of the radio wave.

Critical frequency and virtual height parameters for the sporadic E layer, Es, are labeled as f_oEs and h'Es, respectively, in Figure 3(a). The sporadic E layer is a thin layer of metallic ions of meteoric origins that have been concentrated by wind shears in the neutral atmosphere at E-layer altitudes [30], [31]. In some cases, the Es layer can obscure the E and F ionospheric layer returns, especially at lower frequencies [20].

VERTICAL INCIDENCE SOUNDER IONOGRAM SCALING METHODS AND TECHNIQUES

Research into techniques for automated scaling of VIS ionograms started in the 1960s [18], [19], [32] with a large number of publications during the first decade of the 2000s. This era generated a number of scaling software packages, such as POLAN [4], ARTIST [5], [33], [34], Autoscala [6], [35], [36], and DST-IIP [7], with ARTIST being the most cited. These packages extract and parameterize the key ionogram features.

The approaches investigated for automatic scaling of VIS ionograms can be loosely categorized into four categories: data fitting, template matching, computer vision processing, and ML. Figure 4 presents a taxonomy of the VIS scaling approaches and techniques, including references.

Data fitting and template matching techniques identify key features by exploiting the ionogram trace curved profile, which typically increases as a function of frequency. *Data fitting* involves iteratively fitting a series of polynomial functions (defined through a set of coefficients) to ionogram pixel data points to find trace segments of interest. Ionogram pixel data points that best align with a base polynomial function are deemed as trace candidates. In a similar manner, *template matching* finds VIS traces through a matching operation, but in this case, the baseline fitting functions are derived from empirical data obtained from observed or synthesized ionogram datasets. *Computer vision*-based scaling uses image processing techniques such as edge detection, morphology, filtering, etc., to detect, cluster, and associate pixels for VIS trace identification. *ML*-based methods treat the ionogram feature identification challenge as a closed-box problem. These methods rely on a suitable large training dataset to enable learning of the ionogram semantics. In addition to the aforementioned methods, techniques such as fuzzy logic and the Kalman filter have also been investigated for the scaling of VIS ionograms.

It should be noted that the taxonomy depicted in Figure 4 lists only the different scaling approaches. A review of techniques for ionogram parameterization is not presented in this figure. In many investigations, heuristics are applied to derive the height and frequency parameters of the extracted segments. Furthermore, many, if not all, scaling investigations presented in Figure 4 rely on some form of ionogram preprocessing precursor steps to clean, filter, and smooth the ionogram ahead of ionogram scaling.

SCALING TOOL REVIEW

A short overview of the most common and most cited VIS scaling toolsets is presented in the following sections. This review has found that ARTIST is the most authoritative and mature VIS ionogram scaling tool. Its pedigree has been established through validation on large ionogram datasets

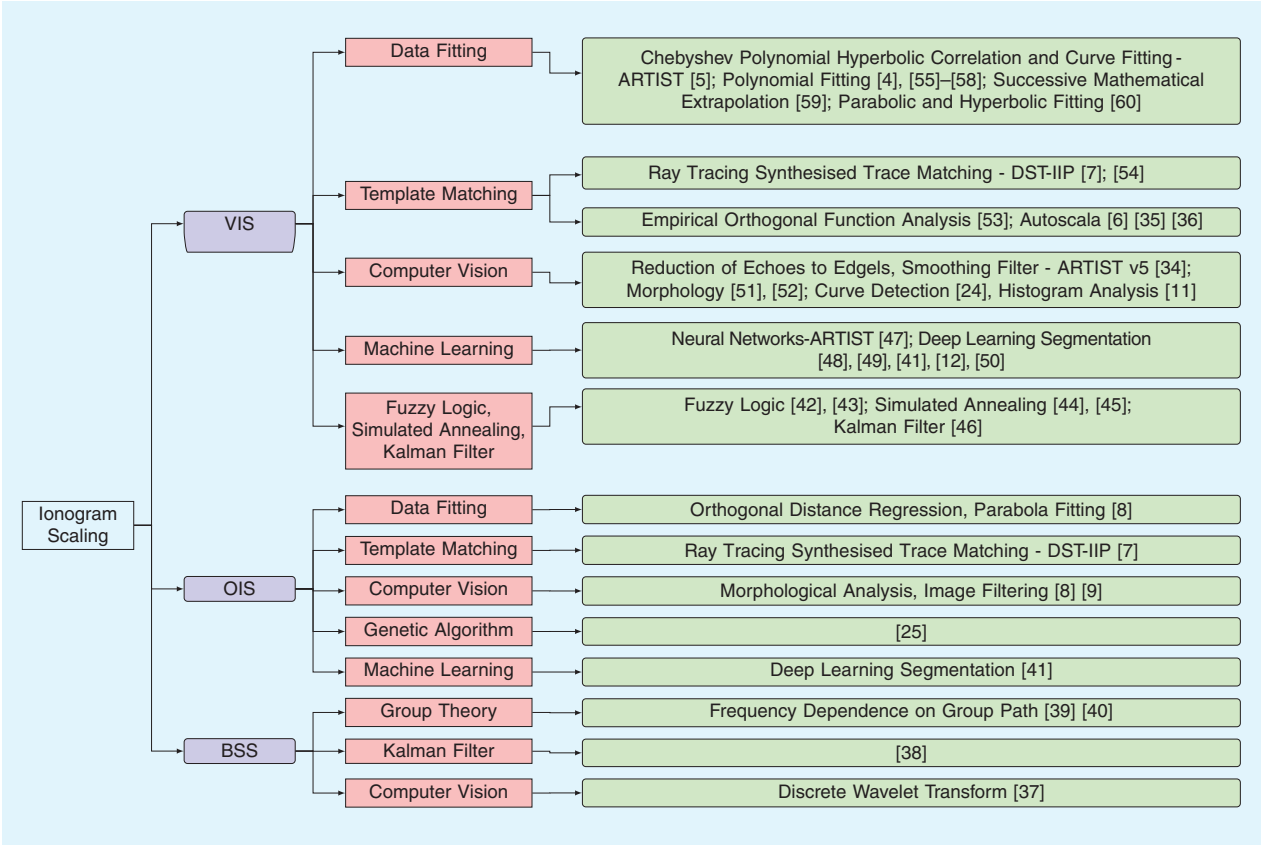

FIGURE 4. The taxonomy for scaling techniques for vertical, oblique, and backscatter ionograms. References are provided for publications investigated in this review.

(tens of thousands) recorded by the GIRO Digisonde network [34], [61]. Furthermore, ARTIST also includes additional information in the scaling output, namely uncertainty and the confidence score, which represent scaling quality and data integrity, respectively. These tool features increase user trust and confidence in the automated scaling solution. Moreover, many automated scaling investigations treat the ARTIST scaling output as an evaluation baseline [12], [62], [63]. Table 1 provides a tabular-based side-by-side comparison of the most popular VIS scaling toolsets.

POLAN

The POLAN software program [4] is a collection of automated scaling techniques that can be applied to VIS ionograms. The program was publicly released as a documented software package in 1985 [4][7]; however, the research into the underlying scaling techniques can be traced back to the prior two decades [55], [56], [57], [58].

POLAN provides the flexibility to implement a range of scaling methods. Techniques such as linear lamination[8] and variable degree polynomial fitting (including overlapping polynomial analysis) can be combined with least squares to perform the scaling operation [4], [65]. POLAN has been used to support the validation of the ARTIST scaled inverted electron density profile for challenging ionogram captures [66], [67].

ARTIST

ARTIST [5], [33], [34], [47] is the most cited automatic scaling technique in the ionospheric literature. It is the most mature and robust automated scaling technique that is used as an evaluation baseline for many scaling investigations.

The ARTIST software has been installed on more than 70 global Digisonde sounder stations [1], [33], [68]. The data[9] from these stations are used to drive the Ionosphere Real Time Assimilative Model (IRTAM) model [69]. Exposure to large datasets sourced from a global network of sounders has been critical to the success of ARTIST.

ARTIST identifies key traces and corresponding parameters in VIS ionograms using hyperbolic fitting. It was found that a hyperbolic polynomial profile matches well with ionogram cusp features, including the F2 ionospheric layer asymptotic cusp feature. See Reinisch and Xueqin [5] for ARTIST scaling algorithm details.

[7] See the GitHub link [64].

[8] This technique processes a pair of ionogram frequency-virtual height data points sequentially to derive the electron density vertical profile. This is in contrast to trace fitting techniques, where the entire ionogram trace is processed in a single step.

[9] ARTIST is deployed as a software application that produces an XML file output that records the scaling parameters and derived electron density profile.

TABLE 1. COMPARATIVE SUMMARY OF POPULAR VIS SCALING TOOLS.

	POLAN	ARTIST	AUTOSCALA	DST-IIP
Era	1980s	1980s +	2000s +	2010s +
Operational use	Unknown	Yes (global Digisonde sounder network)	Yes (AIS INGV Ionosonde)	Yes (JORN)
Year of publication	1975 1985 1988	1983 1998 (version 4) 2004 (version 4.5) 2008 (version 5)	2001 2004 2010	2019
Latitude region(s) applications*	Unknown	Low latitude Mid latitude High latitude	Mid latitude High latitude	Mid latitude
Scaling method(s)	Polynomial fitting	Hyperbolic fitting	Image recognition, correlation	Template matching
O/X polarization data requirement	No	Yes	No	No
Inversion	Yes	Yes	Yes	Yes
Electron density model representation	Polynomial	Chebyshev polynomial	Parameterized model (12 parameters)	QPS (10 parameters)
Uncertainty	No	Yes	No	Yes[†]
Confidence score	No	Yes	No	No

*It is expected that all scaling methods are applicable globally but have been verified only in the listed regions.
[†]Uncertainties reported for the extracted features but not the derived ionospheric parameters.

Early versions of the algorithm exhibited some deficiencies, e.g., incorrect F-layer critical frequency parameterization due to gaps in the F-layer trace caused by spectrum management restriction or interference [33]; poor performance of scaling of ionograms that exhibited ionospheric disturbances, such as spread F [34]; or reliance on polarization tag parameters to differentiate between O and X traces. However, the ARTIST software package has evolved into an operational, reliable, and robust scaling application. Tool enhancements such as reverse inversion,[10] leading edge (LE) detection, and spread F detection have improved the scaling performance of ARTIST [34].

Published ARTIST software release versions subsequent to the initial release [5] include versions 4.0 [33], 4.5 [33], and 5.0 [34]. ARTIST also includes uncertainty and confidence scores as a part of the scaling output. This information is useful for the inference of the quality of the scaling product.

An uncertainty band (95% probability) derived from a statistical analysis of historical data referenced for the sounder station of interest, overlaid on the inverted electron density profile derived from the scaled parameters, gives insight to the operator on how potential scaling errors translate to ionogram inversion output [34]. A confidence score quantifies the quality of the input ionogram in terms of data integrity and detected disturbed ionospheric conditions. This score is useful to infer the reliability of the scaling product. See Conkright and McNamara [70], Galkin et al. [71], and Themens et al. [61], respectively, for more information on the confidence score and results from a study conducted to determine its usefulness.

DST-IIP

The DST-IIP scaling tool [7] is used operationally to support the generation of the Real-Time Ionospheric Model (RTIM) of the Jindalee Operational Radar Network (JORN) in Australia. This tool has been used experimentally since 2006, operationally since 2011, and has been extensively tested on midlatitude ionograms from the Australian region.

The DST-IIP algorithm uses a template matching technique for automatic scaling of both VIS and OIS ionograms. The VIS and OIS scaling algorithms are identical; the VIS is treated as a special case of the OIS where the transmitter and receiver are colocated. The algorithm was designed to be flexible regarding the input ionogram, and so, it can work on ionograms with variable input image quality, thresholded or nonthresholded ionograms, with and without polarization information, and does not require angle of arrival or Doppler information, which is not always available.

The DST-IIP constructs a three-layer electron density profile (E, F1, and F2), defined by 10 parameters used by the JORN RTIM. The quality and uncertainty of the results are reported based on the width of the image features and the similarity of the reproduced ionogram trace created using analytical raytracing through the constructed electron density profile.

First, image preprocessing is performed. This procedure estimates the background noise; applies image cleaning, thresholding, and oblique range transformation algorithms; and then does basic quality checks on the resultant preprocessed image. The oblique range transformation converts the VIS ionogram to an equivalent oblique ionogram where the transmitter and receiver are separated by 500 km. The scaling algorithm then works its way up the traces from the lower ionospheric layers through to the upper layers, making use of the lower layer information as it moves up through the ionosphere. The initial layer parameters are estimated from empirical climatological models. Image processing and fitting are used to extract the E-layer parameters to get the layer height. The F1 layer parameters are based on the climatology. Sporadic-E layer features are extracted directly from the ionogram. F2 layer features are extracted using image processing, and an iterative fitting process is applied to find the electron density profile that best reconstructs the observed ionogram trace. For further

[10] This term describes the practice of using a representative electron density profile to produce an ionogram trace. The reconstructed trace can subsequently be used to assess the validity of the scaled trace and assist with the extrapolation of challenging trace segments.

details on this scaling technique, consult Heitmann and Gardiner-Garden [7].

AUTOSCALA

Autoscala was developed in the early 2000s with the first version being limited to solely scaling the F2 layer feature. A series of improvements was implemented in the same decade to add functionality to scale the F1 [72] and sporadic E [73] layer features and to be robust to ionograms that record weak (faint) traces [36].

Autoscala uses correlation and image recognition techniques (e.g., maximum contrast) [35] to perform automated scaling of VIS ionograms. A suite of representative ionospheric layer traces is iteratively overlaid on an ionogram, and traces that receive the highest correlation score are used to derive the scaling parameters [6]. The fitting procedure uses a pair of traces to detect and scale O and X traces simultaneously. This feature allows the software to scale ionograms recorded by sounders that do not tag traces with polarization information [74].

OBLIQUE INCIDENCE SOUNDERS

The OIS is an HF system that measures the structure of the ionosphere between the transmitter and receiver, which are often separated by 500–3,000 km. An OIS operates similarly to a VIS; it sweeps up in frequency through the HF band and measures the signal strength of the ionospherically propagated radio waves. However, the OIS probes the ionosphere at the midpoint between a transmitter and receiver, while the VIS measures the ionosphere directly above. Figure 5 shows the typical configuration of an OIS system and the oblique propagation path.

An advantage of using an OIS is that it allows for the characterization of the ionosphere at locations where a VIS cannot be installed, such as over bodies of water. In addition, a network of OIS transmit and receive sites[11] allows for the probing of the ionosphere at many more locations than a network of the same number of VIS sites due to the number of combinations of midpoints that can be achieved [75]. Furthermore, the one-way propagation mode feature makes it an attractive ionosphere characterization resource for systems that operate in similar propagation modes, such as HF point-to-point communication systems.

OBLIQUE INCIDENCE SOUNDER IONOGRAM FEATURES

A sample OIS ionogram is presented in Figure 3(b). Similar to the VIS ionogram, the x and y axes of the OIS ionogram are, respectively, frequency and group range. Due to the increase in maximum frequency that the ionosphere can support as a function of the off-zenith angle of the signal [20], OIS ionogram traces have a larger frequency extent than VIS.

Each layer of the ionosphere is able to support two one-hop propagation paths (at different elevation angles) between the spatially separated receiver and transmitter. This means that if it is able to support propagation, each layer of the ionosphere will produce a trace at two group ranges, with the shorter one due to the low elevation path. The two propagation paths attributed to low and high elevation angles are labeled as low and high rays, respectively, in Figure 3(b). At the "nose" feature of the ionogram, the ray paths corresponding to the high and low rays merge, and focusing occurs. This visually distinct feature is a critical OIS scaling parameter known as the *maximum observable frequency* (*MOF*).

The MOF is the most common, and, in many automatic OIS scaling algorithms, the sole feature that is scaled. In addition to being an important parameter for inversion, the MOF feature is useful for frequency management support of HF point-to-point systems.

Similar to the issues that arise when scaling parameters from VIS ionograms in the presence of ionospheric disturbances, scaling the OIS MOF is likewise difficult and potentially prone to error. For example, the presence of a sporadic E layer can render the MOF for the E layer to exceed the MOF for the F layer.

Range-transform techniques may be used to convert the OIS ionogram into an equivalent midpoint VIS ionogram to enable the simple determination of the parameters describing the ionosphere at the midpoint of the oblique path using VIS scaling algorithms. Each pixel of an OIS ionogram (group range and frequency coordinates) corresponds to a specific pixel on the equivalent VIS ionogram (virtual height and frequency coordinates) [20]. This is visually presented in Figure 6. While this technique is often useful and enables ionospheric parameters to be obtained at a location when a VIS cannot be installed, it does make certain assumptions about the ionosphere (spherically symmetric), which introduces errors to the obtained parameters.

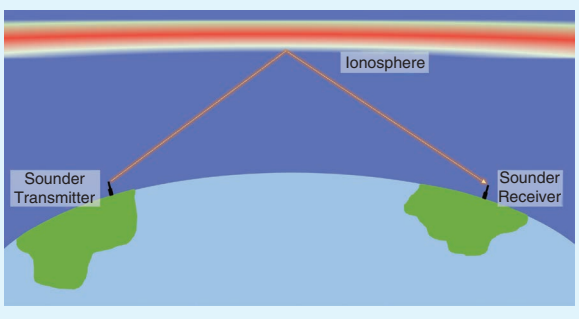

FIGURE 5. A simplified diagram (not to scale) showing OIS operation. Signal reflections from the ionosphere can be used to infer the electron density profile at the midpoint between the transmitter and receiver.

[11]Modern digital receivers can receive multiple OIS transmissions.

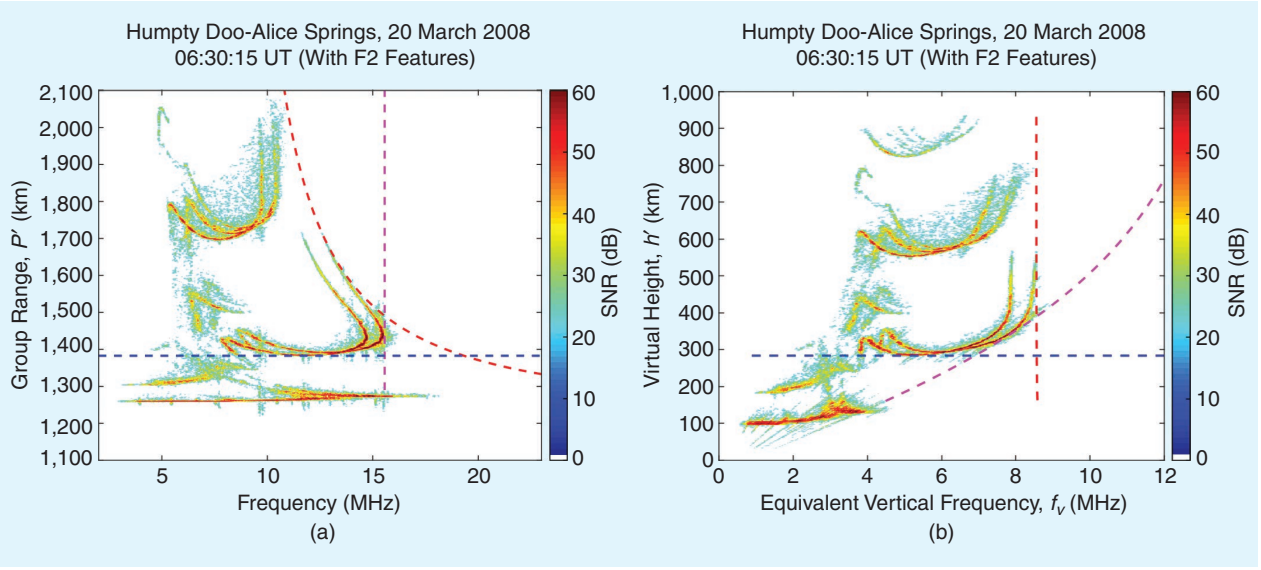

FIGURE 6. Range transformation applied to (a) an OIS ionogram to obtain (b) an equivalent VIS ionogram that can subsequently be used to scale critical frequency (red dashed line) and virtual height (blue dashed line) parameters. (a) An oblique incidence ionogram. (b) An equivalent vertical incidence ionogram. (Source: Generated by DST Group and CoA owned.)

OBLIQUE INCIDENCE SOUNDER IONOGRAM SCALING METHODS AND TECHNIQUES

Traditionally, OISs have been used less often than VISs to characterize the ionosphere, and consequently, research and scaling tool development is less mature. Our review has found that there are fewer publications covering research on scaling techniques for the OIS ionogram in comparison to the VIS ionogram case. The DST-IIP is the most mature OIS scaling tool. A taxonomy of the scaling methodologies presented in Figure 4 summarizes the various OIS scaling algorithms. Trace fitting and image processing are the main techniques.

The DST-IIP scaling software, described in the "Vertical Incidence Sounders" section for scaling VIS ionograms, is also used for the automatic scaling of OIS ionograms. This template matching technique assumes a spherically symmetric ionosphere. A single electron density profile for the midpoint is produced as the final output of the scaling. The F2 layer parameters are fitted using the iterative process of analytical ray tracing and matching the synthetic traces to the observed traces.

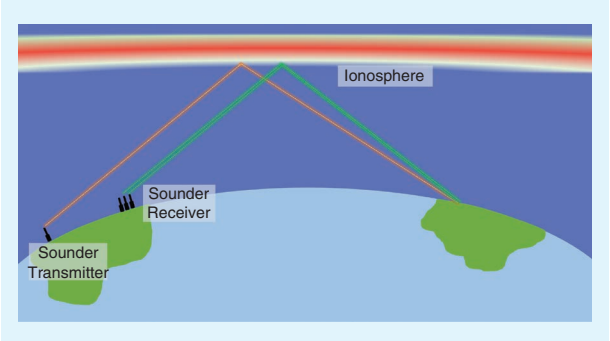

FIGURE 7. A simplified diagram (not to scale) showing BSS operation. Ionospherically propagated radio waves from the transmitter (orange dashed line) are scattered by the ground. The ground back-scattered signal propagates to the receiver via the ionosphere (green dashed line).

BACKSCATTER SOUNDER

The BSS, also known as a *wide sweep backscatter ionogram* (*WSBI*) sounder, is a quasi-monostatic radar system. The transmitter and receiver are separated by a few tens of kilometers for intersite isolation purposes, this being negligible considering the long-range sky-wave propagation distances involved (thousands of kilometers).

The BSS operates similarly to an OTHR. The transmitted signal propagates via the ionosphere to a distant ground location. Most of the energy of the signal is forward scattered; however, a small amount is backscattered and propagates via the ionosphere to the receiver. Figure 7 shows the typical configuration of a BSS and the backscattered propagation path. The BSS provides ionospheric information over a much larger area than the VIS and OIS. Typically, the transmit antenna has a large beamwidth (90°) and so "floodlights" a large area. Reception is on a linear array of antennas, which enables narrow beams to be formed within the transmit coverage. Backscatter ionograms are produced in each of the receiver beams. The BSS requires a much larger transmit power than a VIS or OIS due to the additional losses incurred from the ground scatter and the extra absorption experienced during the double path through the ionosphere. The BSS power requirement is generally of the order of 1 kW to tens of kilowatts, compared to tens of watts for the VIS and OIS. Similar to the VIS and OIS, the BSS sweeps up through frequency in the HF band.

The BSS is an attractive sounder resource for the HF OTHR use case due to the similarities in the propagation paths between the BSS and OTHR. Additionally, physical,

practical, and legal constraints on VIS and OIS sounder transmitter and receiver placement may render the sounder measurement footprints to have limited overlap with OTHR coverage requirements. In these situations, a BSS is more suitable. BSS measurements may support OTHR real-time ionospheric characterization, radar frequency management, and coordinate registration[12] functions [2].

BSS systems are not as widely used as the VIS and OIS due to the additional complexity and cost. The design of each system varies depending on the use case, e.g., the use of a quasi-monostatic system with a continuous waveform or a colocated transmit and receive system using a pulsed waveform must be considered. The quality of the BSS ionogram scales with the transmit power and range-azimuth resolution. Higher power increases the signal-to-noise ratio, which reveals more ionospheric features within the ionograms. This can reveal complications such as contributions from the receive array sidelobes, which may be problematic for automated scaling algorithms.

Some examples of BSS used operationally to support OTHR are the JORN BSS in Australia [2], [21] and the relocatable OTHR (ROTHR) WSBI in the United States [76]. The JORN BSS operates over the frequency range of 5–45 MHz. Two sets of antenna arrays are used to support this: the low (<30-MHz) and high (>30-MHz) band arrays. Transmission is from a vertically polarized log-periodic dipole antenna. Reception is on an array of doublet monopoles, which are able to form beams with appropriate phasing between the receive array elements. The low band transmit system has a transmit power of 10–15 kW, and the high band has a transmit power of 1 kW [2].

The Super Dual Auroral Radar Network (SuperDARN) radars have the ability to operate as a BSS when not operating in their standard data collection mode [77]. Unlike the JORN BSS and ROTHR WSBI, the SuperDARN transmitter and receivers are colocated, and so these radars are pulsed systems. SuperDARN is primarily used for investigating the high-latitude ionosphere by measuring the characteristic returns from ionospheric irregularities. However, ionospheric parameters such as the MOF and f_oF2 can be extracted from the radar ground scatter returns [78].

Some low-power BSS systems have also been developed, such as the Wuhan Ionospheric Oblique Backscattering Sounding System (WIOBSS) [79] and the chirp ionosonde developed by the Institute of Solar-Terrestrial Physics, Siberian Branch of the Russian Academy of Science [39]. These pulsed systems have peak transmit powers of 500 W and 1 kW, respectively.

BACKSCATTER SOUNDER IONOGRAM FEATURES

BSS ionograms display the return signal strength from ground and sea backscatter as a function of sounder transmission frequency and group range. A sample BSS ionogram is presented in Figure 8(a). The LE is a key feature of a BSS ionogram. An LE is a thin ledge-like feature that is visually discernible as a series of connected steep signal strength changes. It is the minimum time delay (group range) for the receipt of the backscattered ionospherically propagated signal as a function of frequency. Multiple LE traces corresponding to propagation via different propagation modes are commonly observed on a BSS ionogram. See Figure 8(a) for samples of key LE traces. The F2 LE may be interpreted as the "nose" or F2 MOF of oblique ionograms formed from receivers positioned on the ground at successive ranges in the direction of the BSS beam. Typically, the LE trace exhibits a smooth and low-order polynomial-like profile with the contour line trending upwards in group range as a function of frequency.

Identification and extraction of LE features in a BSS ionogram is a challenging undertaking. First, the LE is a ledge-like feature with undefined start or end points. It does not resemble visually discernible features, such as cusps, asymptotic lines, or vertices, that are present in VIS and OIS ionograms. Second, the effects of ionospheric dynamics and sounder characteristics can profoundly influence the LE feature. Consequently, the LE may exhibit intensity variation that can render some aspects of the trace line to be faint or disconnected or exhibit localized strong curvature features or "kinks." Third, discrimination logic is required to separate the LE traces based on refractions from different ionospheric layers (including higher-order hops) and magnetoionic splitting. This is complicated by LE traces associated with antenna sidelobe returns [80]. See Figure 8(b) for samples of BSS ionograms that depict the diversity of LE features. Tables 2 and 3, respectively, summarize BSS LE feature characteristics and review the influence of sounder configuration on LE feature composition.

BACKSCATTER SOUNDER IONOGRAM SCALING METHODS AND TECHNIQUES

The BSS is significantly more complex and expensive than VIS and OIS; consequently, they are not as common. In most use cases, a BSS is dedicated to supporting OTHR operation in a specific region and is not treated as an ionospheric sounder resource for contribution to global ionospheric modeling. Not surprisingly, there are no publicly available BSS datasets. Limited access to the BSS system and measurement data has contributed to significantly reduced amounts of research and investigations on automatic scaling of BSS ionograms when compared to VIS and OIS ionograms. This review has found only a few articles that address BSS ionogram LE feature scaling.[13] Figure 4 presents the taxonomy of the approaches for BSS ionogram LE scaling. The application of the Kalman filter and minimum group path theory are the two main approaches used to perform the LE feature extraction. See Figure 4 for references.

IONOGRAM SCALING METRICS

Scaling investigations report performance predominantly using a distance-based metric. A scaling error, defined in

[12]The conversion of the radar group range to a ground location.

[13]It is possible that more publications on this topic exist; however, this review has considered only publications written in English.

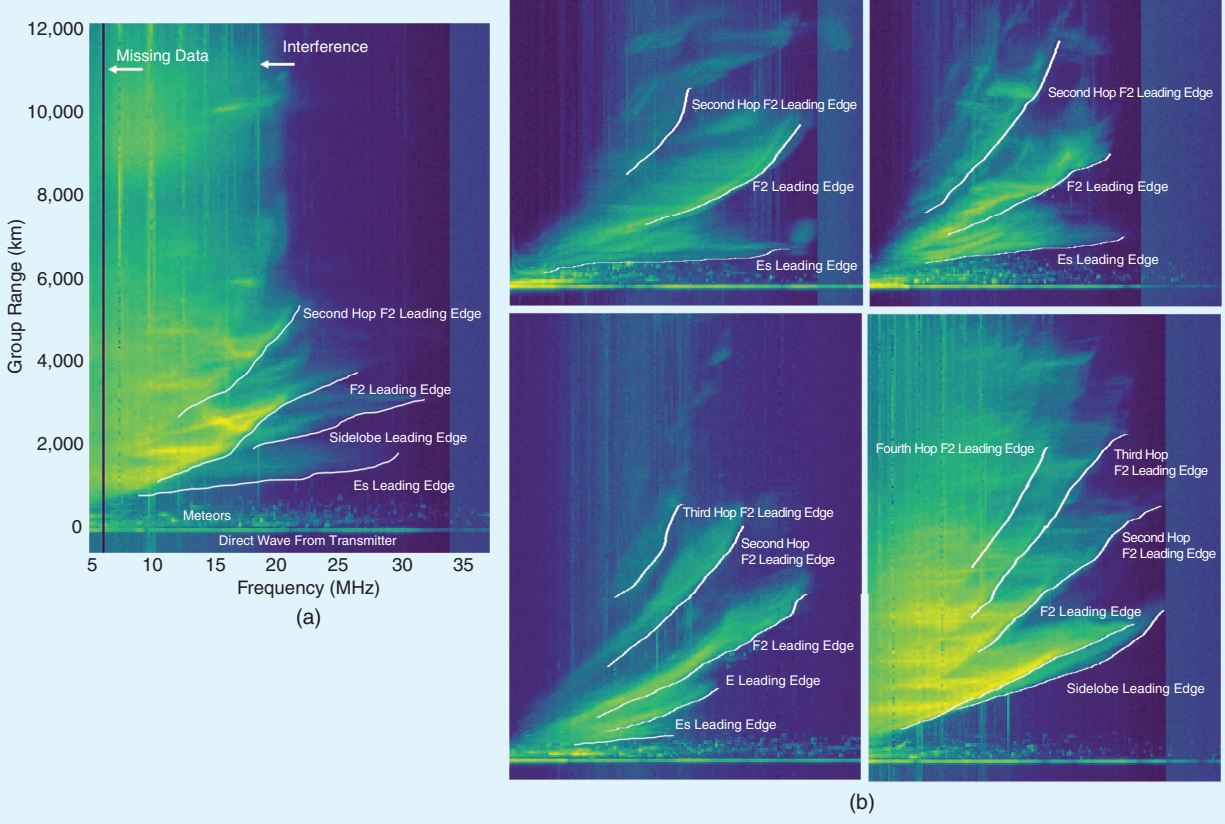

FIGURE 8. BSS ionogram samples. (a) Sample backscatter ionogram with key LE features labeled. Meteoric returns and inference artifacts are also labeled. The F2 LE is of primary interest for the OTHR use case. (b) A sample selection of BSS ionograms with key LE features labeled. The LE features of a BSS ionogram can vary significantly in terms of their return signal strength, start/end positions, length, and shape. Returns from antenna sidelobes and lower ionospheric layers can mask, smear, and complicate the LE feature identification process.

frequency and group range dimensions relative to manually scaled parameters, is used to define the scaling accuracy.

Many VIS and OIS[14] scaling investigations reference the URSI handbook of ionogram scaling [3] for reporting and comparing scaling results. This handbook is recognized as an authoritative standard for the evaluation of VIS scaling performance. The handbook defines the resolution of the scaling error. It is specified in terms of the readability of ionogram features for each ionospheric layer. This parameter defines the error margin for the recognition of accurate and acceptable scaling performance. This readability parameter is referred to as (Δ), and its values are set as follows:

- E layer accuracy (Δ): ± 0.05 MHz, ± 2 km
- F layer accuracy (Δ): ± 0.1 MHz, ± 5 km.

In this handbook, a maximum error of (5Δ) or 20% relative error (whichever is greater) is deemed as acceptable.[15]

Many scaling investigations report scaling performance results specified in terms of both (Δ) and (5Δ). The former is useful for the inference of absolute scaling performance, while the latter is useful for gauging the reliability of ionogram scaling performance, i.e., the evaluation of the ratio of ionogram scaling results that fall within the maximum scaling error allowed.

Some VIS scaling investigations do not reference the URSI handbook and instead report performance using histogram or percentile distribution plots. While this

[14]A dedicated scaling standard for the evaluation of OIS scaling does not exist; however, many investigations adopt the VIS scaling standard [3] for scaling performance evaluation. This practice is deemed acceptable due to the similarity of the features for both ionogram types. The MOF nose vertex of the OIS ionogram is characterized as a distinct feature that can be defined in pixel coordinates, in a similar manner to the cusp features of the VIS ionogram.

[15]The URSI handbook treats these scaling results as doubtful. These scaling results are marked with a qualifying letter to indicate a high level of scaling uncertainty.

TABLE 2. DESCRIPTIONS OF THE LE FEATURES OF A BSS IONOGRAM.

BSS IONOGRAM SCALING FEATURES	DEFINITION AND COMMENTS
F2 LE	The F2 LE feature represents the minimum time delay (group range) for the receipt of a backscatter signal refracted from the F2 ionospheric layer. This feature is labeled in Figure 8(a). The long-range propagation and diurnal stability characteristics of the F2 ionosphere layer make the F2 LE BSS ionogram feature of primary interest for the OTHR use case. Multiple F2 LE traces corresponding to higher-order hops may be observed on some BSS ionograms. The primary (first hop) F2 LE feature is the most visually prominent trace. In many cases, it may be the sole LE feature that can be identified nonambiguously.
F1 LE	The F1 LE feature represents the minimum time delay (group range) for the receipt of a backscatter signal refracted from the F1 ionospheric layer. The F1 LE is usually masked* by the strong F2 layer, and as the F1 layer is absent during nighttime conditions, the F1 LE is not typically observed. For example, this feature is not visible in Figure 8(a).
E LE	The E LE feature represents the minimum time delay (group range) for the receipt of a backscatter signal refracted from the E ionospheric layer. Similar to the F1 LE feature, the E-layer LE is typically masked* by the strong F2 layer and is usually not observed. This feature is not visually discernible in Figure 8(a) but is present in the lower left panel of Figure 8(b).
Es LE	The Es LE feature represents the minimum time delay (group range) for the receipt of a backscatter signal refracted from a sporadic E (Es) layer. This trace is easily identifiable in ionograms due to its unique characteristics in comparison to the E and F traces. The Es trace is visually discernible in ionograms as a relatively flat line that is positioned at low group-range values and spans a wide frequency bandwidth. The Es trace feature is labeled in Figure 8(a).

*The higher level of ionization in the F2 ionospheric layer relative to the lower E and F1 ionospheric layers has the effect of the F2 returns on a BSS ionogram, obscuring the E and F1 LE features.

TABLE 3. THE INFLUENCE OF BSS SOUNDER OPERATIONAL AND DESIGN CHARACTERISTICS ON LE FEATURES OF A BSS IONOGRAM.

BSS SYSTEM CHARACTERISTICS	COMMENTS
Transmitter power, signal processing	Signal-to-noise ratio (SNR) plays a critical role in the definition of the LE feature. Sounder transmit power levels, pulse compression, and integration signal processing techniques influence the SNR of the return signal. In general, a higher SNR produces more distinct BSS ionogram LE features.
Receive antenna pattern (mainlobe)	A narrow receive beamwidth antenna configuration generates higher-resolution ionograms azimuthally. Consequently, the ionograms are sharper with more distinct LE features that are easier to visually identify and interpret. Conversely, a wide beamwidth antenna configuration generates BSS ionogram LE artifacts that are less sharp due to the integration of propagation returns from a larger spatial footprint. For example, the separate LE features corresponding to O and X propagation mode returns are not easily discernible on an ionogram recorded by a BSS configured with a wide receive antenna beamwidth.
Receive antenna pattern (sidelobe)	Backscatter signal returns in the receive antenna sidelobes may produce additional LE features, as shown in Figure 8(a). While the LE features due to sidelobes have lower intensity, they still need to be identified and filtered as part of the scaling process. Additionally, large gradients in the ionosphere during dawn/dusk periods lead to large azimuthal differences in the ionosphere. Thus, a sidelobe return from a direction where the ionosphere is stronger may be falsely identified as the F2 LE if the ionosphere in the direction of the main lobe is significantly weaker.
Multiple beams	BSS systems are typically able to form multiple beams azimuthally. It is expected that there exists a spatial relationship across the beams that can be leveraged to interpret LE features across sequential beams, e.g., backscatter returns detected in a sidelobe in one beam will be detected in the mainlobe of a different beam.

is useful for the analysis of scaling error performance, this format makes it difficult to compare results across investigations.

In contrast to the VIS and OIS case, no standard exists for the evaluation of BSS ionogram scaling. Unlike VIS and OIS, the BSS ionogram exhibits an undefined number of reference features (LE coordinates), and hence, a dedicated evaluation standard is required.

Table 4 provides a summary overview of the ionogram scaling metrics. Note: The metrics presented in Table 4 for the BSS ionogram case represent proposed metrics for consideration based on [40] and [81] but are not recognized as authoritative. See "Recommendation 2: Define and Standardize Metrics for the Evaluation of BSS Ionogram Scaling" in the "Discussion" section for further discussion.

EFFECTS OF SPACE WEATHER ON IONOGRAM FEATURE CHARACTERISTICS

Visual discernment of the critical features in ionograms is complicated by ionospheric irregularities and disturbances, RF interference, and sounder failures. The effects of these phenomena can be observed on an ionogram as distortion, smearing, blurring, or masking of important ionogram features. This increases the complexity of the ionogram scaling process and can lead to ambiguous or misclassification of ionogram features.

TABLE 4. A SUMMARY OF METRICS USED FOR PERFORMANCE EVALUATION OF VIS, OIS, AND BSS IONOGRAMS.

	VIS	OIS	BSS
Feature	E: h′*E*, *foE* F1: h′*F*1 *foF*1 F2: h′*F*2 *foF*2	MOF	Multiple leading-edge points measured in frequency or group range dimension, referenced to a sample surveillance region Applies to all ionospheric layers.
BASELINE	**MANUALLY SCALED FEATURES***		
Absolute error (individual ionogram)	Scaling error wrt frequency and group range		Scaling error wrt frequency or group range Evaluated at each LE point
Minimum accuracy (individual ionogram)	E layer ± 0.05 MHz, ± 2 km F layer: ± 0.1 MHz, ± 5 km (based on URSI handbook)		E layer ± xxMHz or ± xxkm F layer: ± xxMHz or ± xx km Evaluated at each LE point
Acceptable accuracy (individual ionogram)	E layer ± 0.25 MHz, ± 10 km F layer: ± 0.5 MHz, ± 25 km (based on URSI handbook)		E layer ± xxMHz or ± xxkm F layer: ± xxMHz or ± xx km Evaluated at each LE point
Scaling performance reporting – accuracy (whole dataset)	Ratio (percentage) of ionograms that satisfy minimum/acceptable accuracy; reported for each feature.		Ratio of estimated LE data points that satisfy minimum/acceptable accuracy; reported for each ionospheric layer
Scaling performance reporting – recall (whole dataset)	Ratio (percentage) of ionograms for which no features are estimated; reported for each feature.		Ratio of LE data points for which no estimates are generated; reported for each ionospheric layer

*This can also be scaling results obtained from an alternate scaling tool if comparison is performed across toolsets.
Note: No authoritative metrics exist for BSS ionogram evaluation. BSS metrics, displayed as orange cells, are the proposed metrics for consideration.

TABLE 5. A SUMMARY OF THE INFLUENCE OF SOLAR VARIABILITY ON IONOGRAM FEATURE CHARACTERISTICS.

VARIABILITY FEATURE	TIMESCALE	SPATIAL SCALE	COMMENTS
Diurnal	24 h	Global	Higher levels of ionization occur during the day versus night. The E and F1 layers disappear at night, leaving only a weakened F2 layer. Consequently, nighttime ionograms do not have traces corresponding to the E and F1 layers. See Davies [20].
Sunrise and sunset	Minutes	Global	Passage of the dawn and dusk terminators results in highly dynamic transformations of the ionosphere [13]. This imposes strong Doppler shifts on the radio wave signal, which will be apparent on sounders that measure Doppler, such as the Digisonde.
Seasonal	One to three months	Global	The level of ionization varies significantly with season. The E and F1 layers are strongest in summer and weakest in winter. However, during the day, and especially in the Northern Hemisphere, the F2 layer is stronger in the winter than in the summer (the winter anomaly) [20]. This is due to slower ion loss processes in the winter F2 layer.
Solar cycle	11 years	Global	Solar activity varies periodically in cycles of approximately 11 years. In general, higher frequency values for ionospheric layer trace returns are observed near the peak of the solar cycle [20].
Latitudinal	N/A	Thousands of km	The strength of the ionosphere varies significantly with latitude. The strength of the E and F1 layers peaks at the subsolar latitude near the equator, whereas the F2 layer strength peaks at approximately 15° north and south of the geomagnetic equator, known as the *Appleton Anomaly regions* [20].

N/A: not applicable.

In these situations, a trained human (SME) is required to make sound judgment, and interpolation and/or extrapolation are often required to complete the feature interpretation process. Tables 5 and 6 provide a summary of the ionospheric disturbances and interference effects and how they affect ionogram feature characteristics.

REVIEW OF DEEP LEARNING IONOGRAM SCALING INVESTIGATIONS

There is a growing interest in the application of ML to ionogram scaling. The majority of current investigations have been predominantly applied to VIS ionograms [12], [41], [49]. ML, specifically deep learning convolutional and Transformer methods, offers a powerful feature extraction capability [82] that can be leveraged for automated ionogram scaling.

Mochalov and Mochalova [48] is the first investigation that applies a convolutional U-Net model for the extraction of traces pertaining to E, F1, and F2 ionospheric layer reflections in a VIS ionogram. The investigation by De La Jara and Olivares [49] improves on the results of Mochalov and Mochalova [48] by fine-tuning a convolutional encoder-decoder model pretrained on trace features derived using filtering, clustering, and mean shift techniques. The investigation by Xiao et al. [12] experiments with different convolutional backbones in the Feature Pyramid Network architecture.

TABLE 6. A SUMMARY OF THE EFFECTS OF NATURAL PHENOMENA ON IONOGRAM CHARACTERISTICS.

IRREGULARITY FEATURE	TIME SCALE	SPATIAL SCALE	COMMENTS
Sporadic E (Es)	Hours	Tens to hundreds of km	The sporadic E layer, Es, is a thin layer of concentrated metallic ions. Additional traces and features will be evident in VIS, OIS, and BSS ionograms. In some cases, the Es layer can obscure the F-layer returns in VIS ionograms, especially at lower frequencies.
Meteor	Seconds	Small	Reflections from transient meteors manifest on an ionogram at low group ranges. These returns are easily identifiable and able to be separated from the main ionospheric layer returns. However, in some cases, they can contribute to ionogram feature and propagation mode classification issues [7].
Solar flare	Minutes to hours	Large	Intense short-term bursts of X-rays originating from solar flares significantly increase the strength of the D layer of the ionosphere, resulting in enhanced absorption of HF radio waves. Consequently, a portion of, or in some extreme cases, the complete HF band can be "blocked" out for HF propagation. Aspects of—or the entire—ionospheric layer returns can be masked out on an ionogram recording.
Ionospheric irregularities	N/A	Thousands of km	Ionospheric electrodynamics vary as a function of geomagnetic location (equatorial, midlatitude, and auroral/polar). Ionospheric irregularities may occur in each of these regions and are due to different electrodynamic processes. The irregularities can cause range and/or frequency spreading of the signal. When the F layer returns are affected, this is referred to as spread F.
Small-scale TID (SSTID)	Minutes	Tens of km	SSTIDs may have a large effect on ionospheric soundings, with very complicated multiple oscillatory and "splitting" features in the ionogram traces being evident [13]. Very-small-scale SSTIDs (~25 km) may cause spread F [13].
Medium-scale TID (MSTID)	Minutes	Hundreds of km	MSTIDs may be generated by atmospheric gravity waves in the neutral atmosphere, perturbing the ionospheric plasma, or by electrodynamic processes within the ionosphere. They cause additional cusp or "loop" features in VIS ionograms [83] and complex curve features (or "kinks") in OIS ionograms [84] and introduce additional LEs in BSS ionograms [80].
Large-scale TID (LSTID)	Hours	Thousands of km	LSTIDs, generated primarily in the auroral regions, cause the ionosphere to vary slowly. The effect of LSTIDs is not noticeable at the resolution of a single VIS ionogram. Analysis of a series of VIS ionograms is required to confirm a pattern of virtual height and critical frequency variations due to LSTIDs [85]. Consequently, LSTIDs do not pose a problem for the scaling of VIS ionograms. However, strong LSTIDs may cause additional oblique propagation paths, which manifest as additional "satellite" traces on OIS ionograms [84] and pose a challenge for automated scaling algorithms.
Chordal modes	N/A	N/A	Steep gradients in the equatorial ionosphere can affect propagation path characteristics for north-south-oriented paths. In these cases, the sounder transmission signals may not follow a "direct" path from the transmitter to the receiver (OIS) or ground (BSS) via the ionosphere but rather follow a more complicated path where the radio waves "skip" across the geomagnetic equator between the north and south equatorial Appleton Anomaly regions [13]. This phenomenon enables propagation over long distances. Chordal propagation modes manifest on BSS ionograms as isolated strong echoes at long group ranges.

This investigation achieves a high performance with reported precision and recall of 98% and 90%, respectively.

Importantly, in addition to reporting scaling performance using computer vision metrics, the results presented by [12] are also conveyed in ionogram domain metrics; frequency and group range error are reported for the scaled critical trace parameters. The scaling performance reported by Xiao et al. [12] exceeds the scaling results obtained using ARTIST for the dataset under investigation.

The work of Xue et al. [41] is, to our best knowledge, the only work that applies deep learning to all three ionogram types. In their investigation, separate convolutional models were used to perform ionogram classification (VIS, OIS, or BSS) and trace segmentation. The results reported by Xue et al.[41] are provided only for the classification model, and hence, a comparative performance assessment of feature extraction cannot be undertaken.

To the best of our knowledge, no investigations have been conducted for the application of Transformer-based models for ionogram scaling applications. Visual Transformer models have surpassed the performance of convolutional models for image classification[16] and therefore should be reviewed for ionogram scaling applications, particularly for the OIS and BSS categories for which limited scaling solutions are available. This represents an opportunity for further research.

DISCUSSION

This section includes a discussion of insights, findings, and recommendations based on the literature review conducted for ionogram scaling. This material can be used to guide and stimulate further research in this field.

Finding 1: Lack of an Ionogram Benchmark Dataset

The success of deep learning is largely attributed to the availability of publicly available benchmark datasets. For

[16]See https://web.archive.org/web/20250414093559/https:/paperswithcode.com/sota/image-classification-on-imagenet for a leaderboard snapshot of image classification models evaluated against the ImageNet benchmark dataset.

example, the Cityscapes dataset [86] is a large collection of images relating to urban street scenes that includes pixel-level annotations. This dataset is commonly used to measure, report, and compare deep learning segmentation model performance. Our review has found that an equivalent benchmark dataset does not exist for ionogram scaling. Fair and transparent comparative evaluation of automatic ionogram scaling techniques and algorithms is difficult to perform due to the lack of a benchmark dataset. Ionogram scaling publications reference custom datasets that vary in data size and diversity and are seldom publicly available.

Recommendation 1: The Development of an Ionogram Scaling Benchmark Dataset

An authoritative ionogram scaling benchmark dataset should be developed. This dataset should encompass all three sounder types to address the unique ionogram characteristics pertaining to each. Resources such as Reinisch and Galkin [1] can be leveraged to accelerate this effort.

Some factors to be considered in the design of an ionogram scaling benchmark dataset include the following:

- *Manual scaling of labels should be authored by a group of SMEs with a diverse ionogram scaling experience.* Ionogram scaling labels need to account for the subjective interpretation nature of the ionogram feature set, and hence, a diverse composition of scaling experience is encouraged for the benchmark dataset. This is particularly important for the labeling of ionograms displaying the effects of ionospheric disturbances and ionograms recorded by a BSS sounder in general.
- *Include labels generated by authoritative scaling tools.* The inclusion of labels generated by authoritative scaling tools (where such tools are available, e.g., ARTIST for VIS ionograms) will enable a transparent and repeatable comparative scaling performance evaluation of scaling techniques.
- *Strive for a diverse and balanced dataset design.* The variability of the ionosphere is well known, and studies such as [39], [80], and [87] show that less than 10% of ionograms can be described as originating from "quiet" ionospheric conditions. Consequently, a benchmark dataset should be composed of a balanced and diverse composition of ionograms. Space weather variability and irregularity factors, as described in Tables 5 and 6, can be used to guide the design of a benchmark dataset.

The dataset should also include metadata that describe the inferred ionosphere conditions and sounder configuration parameters referenced for each ionogram. This information is valuable for informed scaling model performance assessment, including model generalization. See Galkin et al. [88] for an analysis of metadata requirements for an Internet ionospheric data repository. In addition, this information can also be used to enable the implementation of class weighting approaches [89] during model development to compensate for unbalanced datasets. The convention adopted by ARTIST [71] for the evaluation and reporting of ionogram data quality for VIS ionograms can be used as an exemplar and be expanded to cover OIS and BSS ionogram datasets.

Finding 2: Lack of a Scaling Standard for the BSS Ionogram

The URSI scaling standard [3] defines metrics for the evaluation of VIS ionogram scaling performance. The metrics are defined in terms of acceptability and accuracy referenced to frequency and group range dimensions (discussed earlier in the "Vertical Incidence Sounders" section) and are very useful for gauging and comparing automatic scaling performance. The vast majority of VIS scaling investigations use these metrics for reporting scaling performance.

While no official scaling standard is defined for OIS ionograms, the VIS scaling standard [3] is commonly referenced in OIS scaling investigations. This practice is deemed acceptable due to the similarity of OIS and VIS trace feature characteristics. No equivalent scaling standard exists for the evaluation of BSS ionogram scaling performance. Without such a standard, existing BSS scaling investigations report performance using custom metrics.

Recommendation 2: Define and Standardize Metrics for the Evaluation of BSS Ionogram Scaling

The LE features of a BSS ionogram do not resemble the features embedded in VIS and OIS ionograms; hence, a dedicated scaling standard is required. An obvious metric is based on the pixel-wise distance between the estimated and truth (manually labeled) LE traces for each ionospheric layer return. This distance can be reported in frequency and/or group range dimensions. Given that a BSS ionogram LE trace exhibits an undefined length with no fixed start or end coordinates, a decision needs to be made on how many and which LE pixels should be used as reference pixels for metric calculations.

One approach to resolve this dilemma is to divide the LE trace into a fixed number of equally spaced segments and use the pixel coordinates of each segment for evaluation purposes. One disadvantage of this technique is that the coordinates of each reference pixel will vary from one ionogram to another due to the differences in the LE trace profile (trace length and start and end coordinates). This will render the evaluation mechanism unrepeatable across datasets. An alternative approach is to select a fixed number of evaluation coordinates, defined in group-range or frequency dimensions, and use these coordinates as reference points for evaluation purposes. This approach is used by Song et al. [40] and Crouch [81], where five predefined identical frequency and group-range values, respectively, are used to evaluate the distance of the estimated LE trace to truth across the full dataset. Figure 9 depicts this metric approach for a sample BSS ionogram. The benefit of this approach is that the reference LE pixels are identical across the ionograms, and this enables a repeatable and transparent evaluation. A potential problem with this proposed technique is that it is not guaranteed that an LE trace will coincide with all group-range reference values (i.e., the LE trace may not extend across the span of group range represented by the reference values). In

this situation, the associated reference group-range value can be omitted during metric calculations.

It is recommended that the URSI scaling standard [3] for reporting scaling performance in terms of the ratio of results that are deemed as accurate and acceptable (based on error margins, as discussed earlier in the "Vertical Incidence Sounders" section) is also adopted for reporting BSS scaling performance. In addition to including metrics that report scaling performance in terms of accuracy, metrics that account for the recall rate, i.e., the ratio of LE pixels that were not found by the LE extraction model (false negatives), should also be considered.

Recommendation 3: Conduct an Experimental Study to Evaluate, Compare, and Demonstrate the Effectiveness of Scaling Methods and Techniques

An experimental-based case study comparing ionogram scaling solutions generated by a suite of scaling tools and methods would be extremely useful to the ionospheric research community. Some reviews of this nature have been performed for a pairwise assessment of VIS scaling tools, e.g., ARTIST versus Autoscala [62], [63]. However, to the best of our knowledge, no comparative experimental studies have been performed across all sounder types. This study should evaluate scaling tools and methods in multiple geographical locations and ionospheric conditions.

Recommendation 4: Continue Research on Deep Learning Techniques for Automatic Ionogram Scaling

The transformation of image semantics contextualized by human experience in a scientific domain into a set of instructions that can be coded with a programming language is extremely challenging. The subjective interpretation aspect and requirement to codify all possible edge cases and domain-specific nuances render the task of automated software solutions that produce accurate and repeatable outcomes at scale without human intervention almost impossible to achieve. The recent advent of deep learning can address some aspects of this challenge.

Deep learning has made noteworthy advancements over the last decade to achieve a high level of success in computer vision tasks such as image recognition, object detection, and image segmentation. Segmentation, a pixel-level classification of an image into semantic regions of interest, is of particular relevance to ionogram scaling. Convolutional [90], and recently, Transformer-based methods [91], are utilized to develop state-of-the-art image segmentation models that are producing remarkable performance against open source benchmark image datasets.

Ionogram scaling can benefit from the ability of deep learning segmentation models to learn salient spatial relationships at local and global scales related to pixel intensity, edges, contours, and shapes in an ionogram image. This capability can be particularly useful for the scaling of ionograms that are captured in disturbed ionospheric conditions, where image features can be occluded, distorted, or separated. Moreover, the challenge of the identification of LE features in a BSS ionogram may not be adequately satisfied through the use of conventional techniques that have been successful for VIS and OIS ionograms. For this case, the adoption of deep learning segmentation methodologies may be the most beneficial.

Opportunities for research on deep learning segmentation models for automatic ionogram scaling applications include, but are not limited to, the following:

- *Application of Vision Transformer models for ionogram feature extraction.* Transformer model design has demonstrated a performance edge over convolutional-based models in the computer vision domain.
- *Use of semisupervised and self-supervised segmentation model designs, transfer learning, and/or custom data augmentation techniques.* These approaches can alleviate the dataset labeling burden.
- *Integration of radio wave propagation theory and ionospheric physics with deep learning.* This approach can be used to produce a physics-guided deep learning ionogram scaling model.

It is anticipated that the release of annotated ionogram scaling datasets will accelerate the research of deep learning for application to ionogram scaling. Data science competitions, such as Kaggle [92], have stimulated deep learning research for diverse applications through the use of large open source datasets.

CONCLUSION

The ionosphere is a highly dynamic medium; hence, characterization of the ionosphere is crucial for the effective operation of any HF system. Vertical sounders, oblique sounders,

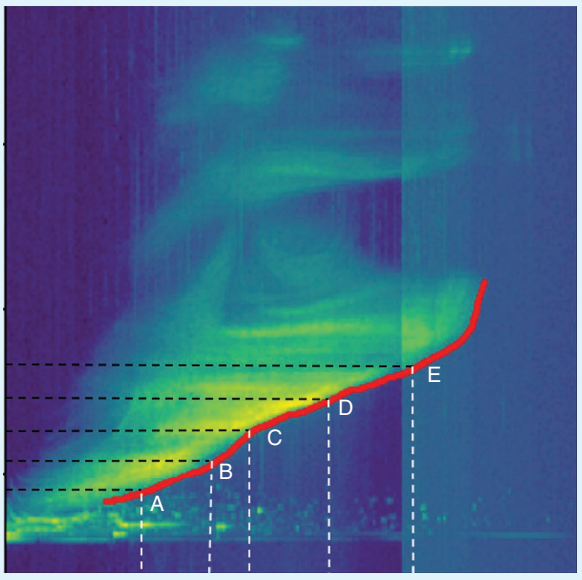

FIGURE 9. This diagram displays one approach that can be adopted for standardizing BSS scaling performance evaluation. A set of five group-range lines (dashed black lines) is used to derive five unique LE reference pixel coordinates (labeled as A–E) that can be used to quantify the frequency scaling error (dashed white lines) obtained from an LE extraction model.

and BSSs are used to record bottom-side measurements of the ionosphere to enable the quantification of its properties. The task of analyzing, identifying, and extracting features from ionospheric measurements (ionograms), known as *scaling*, is a time intensive and laborious process, and so, a number of automated scaling techniques and tools have been developed over the last few decades. The proliferation of vertical sounder networks globally has stimulated the research and development of scaling algorithms for the vertical sounder, and hence, it is not surprising that the majority of publications focus on the vertical sounder application.

In this article, we have reviewed the techniques for automated scaling across all ground-based ionospheric sounder systems. To the best of our knowledge, this is the first comparative review across all sounder types. A review of ionogram features, toolsets, and metrics for each sounder is presented. In addition, an analysis of the impact of ionospheric irregularities and disturbances on the ionogram scaling challenge is also included.

Furthermore, we have included a discussion of our findings and recommendations that we hope will accelerate reproducible research in this field to expedite progress for the automated scaling of ionograms recorded by all types of sounder systems. We believe that the development of an ionogram scaling benchmark dataset and metric standardization will stimulate further research in this field and draw participation from the deep learning community. This can be particularly beneficial for the oblique and BSS systems for which there are a limited number of automated scaling solutions available.

An automated scaling ionogram capability enables the real-time characterization and forecasting of ionospheric properties derived from large global ionospheric datasets recorded by vertical, oblique, and BSS systems. This is a crucial requirement for supporting HF systems that exploit the ionosphere to provide a beyond-line-of-sight capability, such as communications, surveillance, navigation, and remote sensing.

ACKNOWLEDGMENT

We thank Lenard Pederick, Andrew Heitmann, and David Holdsworth for useful discussions, reviews, and suggestions related to writing this article. We thank Lenard Pederick for generating Figure 3. We thank Andrew Heitmann for generating Figures 1 and 6.

AUTHOR INFORMATION

Rafal Sienicki (rafal.sienicki@defence.gov.au) received his B.E. degree in computer systems engineering from the University of South Australia in 2002. In 2005, he joined the Defence Science and Technology Group, Edinburgh, SA 5111 Australia, where he is currently a research scientist. He is currently pursuing his Ph.D. degree at the University of Sydney. His research interests include modeling, simulation and experimentation, electronic warfare, radar, and machine learning.

Danielle J. Edwards (danielle.edwards@defence.gov.au) received her B.Sc. degree in experimental and theoretical physics and her M.Phil. degree in physics from the University of Adelaide, Adelaide, SA, Australia, in 2018 and 2021, respectively. Since 2019, she has been a physicist with the High Frequency Systems Group, Defence Science and Technology Group, Edinburgh, SA 5111 Australia. Her research interests include ionospheric physics, the propagation of high-frequency radio waves, and performance modeling of over-the-horizon radar.

Manuel A. Cervera (manuel.cervera@defence.gov.au) received his B.Sc. (Hons.) and Ph.D. degrees from the Physics Department, the University of Adelaide, Adelaide, SA, Australia, in 1990 and 1996, respectively. He is a senior scientist and the discipline leader for HF Radar Performance and Environment in the HF Systems Science and Technology Capability Area at the Defence Science and Technology Group, Edinburgh, SA 5111 Australia. Since 2018, he has also been an adjunct associate professor with the Space and Atmospheric Physics Group, School of Physical Sciences, the University of Adelaide, Adelaide, SA 5005 Australia. His research interests include ionospheric physics, radio wave propagation through the ionosphere, HF radio systems, and performance modeling of over-the-horizon radar.

Philip H. W. Leong (philip.leong@sydney.edu.au) received his B.Sc., B.E., and Ph.D. degrees from the University of Sydney. From 1997 to 2009, he was with the Chinese University of Hong Kong. He is currently a professor of computer systems in the School of Electrical and Computer Engineering at the University of Sydney, Sydney NSW 2006, Australia, chief technology officer at CruxML, and chief executive officer at TernaryNet. His research interests include field-programmable gate array architectures and applications, computer architecture, and machine learning.

REFERENCES

[1] B. W. Reinisch and I. A. Galkin, "Global ionospheric radio observatory (GIRO)," *Earth Planets Space*, vol. 63, no. 4, pp. 377–381, 2011, doi: 10.5047/eps.2011.03.001.

[2] G. F. Earl and B. D. Ward, "The frequency management system of the Jindalee over-the-horizon backscatter HF radar," *Radio Sci.*, vol. 22, no. 2, pp. 275–291, 1987. [Online]. Available: https://agupubs.onlinelibrary.wiley.com/doi/abs/10.1029/RS022i002p00275

[3] W. R. Piggott and K. Rawer, "U.R.S.I. handbook of ionogram interpretation and reduction," Nat. Acad. of Sci., Washington, DC, USA, 1978. [Online]. Available: https://repository.library.noaa.gov/view/noaa/10404

[4] J. E. Titheridge, "Ionogram analysis with the generalised program POLAN," Nat. Acad. of Sci., Washington, DC, USA, Dec. 1985. [Online]. Available: https://repository.library.noaa.gov/view/noaa/1343

[5] B. W. Reinisch and H. Xueqin, "Automatic calculation of electron density profiles from digital ionograms: 3. Processing of bottomside ionograms," *Radio Sci.*, vol. 18, no. 3, pp. 477–492, May 1983, doi: 10.1029/RS018i003p00477.

[6] C. Scotto, "A method for processing ionograms based on correlation technique," *Phys. Chem. Earth. Part C*, vol. 26, no. 5, pp. 367–371, Jan. 2001, doi: 10.1016/S1464-1917(01)00015-0. [Online]. Available: https://www.sciencedirect.com/science/article/pii/S1464191701000150

[7] A. J. Heitmann and R. S. Gardiner-Garden, "A robust feature extraction and parameterized fitting algorithm for bottom-side oblique and vertical incidence ionograms," *Radio Sci.*, vol. 54, no. 1, pp. 115–134, Jan. 2019, doi: 10.1029/2018RS006682.

[8] N. J. Redding, "Image understanding of oblique ionograms: The autoscaling problem," in *Proc. Aust. New Zealand Conf. Intell. Inf. Syst. (ANZIIS)*, 1996, pp. 155–160, doi: 10.1109/ANZIIS.1996.573922.

[9] Y. Hu, H. Song, X. Zou, and Z. Zhao, "Real-time automatic scaling method of oblique ionogram parameters based on morphological operator and inversion technique," *Wuhan Univ. J. Natural Sci.*, vol. 20, no. 4, pp. 323–328, 2015, doi: 10.1007/s11859-015-1100-2.

[10] A. Ippolito, C. Scotto, D. Sabbagh, V. Sgrigna, and P. Maher, "A procedure for the reliability improvement of the oblique ionograms automatic scaling algorithm," *Radio Sci.*, vol. 51, no. 5, pp. 454–460, 2016, doi: 10.1002/2015RS005919.

[11] K. J. W. Lynn, "Histogram-based ionogram displays and their application to autoscaling," *Adv. Space Res.*, vol. 61, no. 5, pp. 1220–1229, Mar. 2018, doi: 10.1016/j.asr.2017.12.019. [Online]. Available: https://www.sciencedirect.com/science/article/pii/S0273117717308955

[12] Z. Xiao, J. Wang, J. Li, B. Zhao, L. Hu, and L. Liu, "Deep-learning for ionogram automatic scaling," *Adv. Space Res.*, vol. 66, no. 4, pp. 942–950, 2020, doi: 10.1016/j.asr.2020.05.009. [Online]. Available: https://www.sciencedirect.com/science/article/pii/S027311772030332X

[13] M. A. Cervera, T. J. Harris, D. A. Holdsworth, and D. J. Netherway, "Ionospheric effects on HF radio wave propagation," in *Ionosphere Dynamics and Applications* (Geophysical Monograph Series), C. Huang, G. Lu, Y. Zhang, and L. J. Paxton, Eds., Hoboken, NJ, USA: AGU, 2021, pp. 439–492, doi: 10.1002/9781119815617.ch19.

[14] P. L. Dyson and J. A. Bennett, "A model of the vertical distribution of the electron concentration in the ionosphere and its application to oblique propagation studies," *J. Atmos. Terr. Phys.*, vol. 50, no. 3, pp. 251–262, 1988, doi: 10.1016/0021-9169(88)90074-8. [Online]. Available: https://www.sciencedirect.com/science/article/pii/0021916988900748

[15] R. Gardiner-Garden, A. Heitmann, and N. Brett, "A parametric model of the ionospheris electron density profile for JORN," Nat. Secur. and ISR Division, Edinburgh, U.K., DST-Group-TN-1722, Dec. 2018. [Online]. Available: https://www.dst.defence.gov.au/sites/default/files/publications/documents/DST-Group-TN-1722.pdf

[16] R. D. Hunsucker, *Radio Techniques for Probing the Terrestrial Ionosphere* (Physics and Chemistry Space), vol. 22. Berlin, Heidelberg, Germany: Springer-Verlag, 1991.

[17] J. W. Wright and L. A. Fine, "Mean electron density variations of the quiet ionosphere 2 - April 1959," U. S. Dept. of Commerce, Washington, DC, USA, Feb. 1960. [Online]. Available: https://nvlpubs.nist.gov/nistpubs/Legacy/TN/nbstechnicalnote40-1.pdf

[18] J. R. Doupnik and E. R. Schmerling, "The reduction of ionograms from the bottomside and topside," *J. Atmos. Terr. Phys.*, vol. 27, no. 8, pp. 917–941, 1965, doi: 10.1016/0021-9169(65)90027-9. [Online]. Available: https://www.sciencedirect.com/science/article/pii/0021916965900279

[19] W. Becker, "On the manual and digital computer methods used at Lindau for the conversion of multifrequency ionograms to electron density-height profiles," *Radio Sci.*, vol. 2, no. 10, pp. 1205–1232, Oct. 1967, doi: 10.1002/rds19672101205.

[20] K. Davies, *Ionospheric Radio*. London, U.K.: IET, 1990, doi: 10.1049/PBEW031E.

[21] D. J. Netherway, M. J. Whitington, and R. S. Gardiner-Garden, "High range resolution backscatter sounder ionograms," Nat. Secur. and ISR Division, Edinburgh, U.K., DST-Group-TR-3477, 2018.

[22] F. Arıkan, O. Arıkan, and S. Salous, "A new algorithm for high-quality ionogram generation and analysis," *Radio Sci.*, vol. 37, no. 1, pp. 1–11, 2002. [Online]. Available: https://agupubs.onlinelibrary.wiley.com/doi/abs/10.1029/2000RS002569,eprint=https://agupubs.onlinelibrary.wiley.com/doi/pdf/10.1029/2000RS002569

[23] N. Theera-Umpon, "Ionospheric F-layer critical frequency estimation from digital ionogram analysis," in *Proc. Int. Conf. Comput. Sci. Its Appl.*, 2007, pp. 190–200.

[24] M. Fagre et al., "Algorithm for automatic scaling of the F-layer using image processing of ionograms," *IEEE Trans. Geosci. Remote Sens.*, vol. 59, no. 1, pp. 220–227, Jan. 2021, doi: 10.1109/TGRS.2020.2996405.

[25] H. Song, Y. Hu, C. Jiang, C. Zhou, Z. Zhao, and X. Zou, "An automatic scaling method for obtaining the trace and parameters from oblique ionogram based on hybrid genetic algorithm," *Radio Sci.*, vol. 51, no. 12, pp. 1838–1854, 2016, doi: 10.1002/2016RS005987.

[26] T. J. Harris, A. D. Quinn, and L. H. Pederick, "The DST group ionospheric sounder replacement for JORN," *Radio Sci.*, vol. 51, no. 6, pp. 563–572, 2016, doi: 10.1002/2015RS005881.

[27] "Scaled ionosheric data format," Australian Space Weather Forecasting Centre, Adelaide, Australia, 2022. [Online]. Available: https://www.sws.bom.gov.au/World_Data_Centre/2/8/1

[28] T. Maruyama et al., "Low latitude ionosphere-thermosphere dynamics studies with inosonde chain in Southeast Asia," *Ann. Geophys.*, vol. 25, no. 7, pp. 1569–1577, 2007, doi: 10.5194/angeo-25-1569-2007. [Online]. Available: https://angeo.copernicus.org/articles/25/1569/2007/

[29] S. C. Gladden, L. Central Radio Propagation, L. Boulder, and S. United, "A history of vertical-incidence ionsphere sounding at the National Bureau of Standards," U.S. Dept. of Commerce, Washington, DC, USA, 1959. [Online]. Available: https://www.govinfo.gov/content/pkg/GOVPUB-C13-e4f91b98a62d26a7a67171a1d92d7f3d/pdf/GOVPUB-C13-e4f91b98a62d26a7a67171a1d92d7f3d.pdf

[30] J. D. Whitehead, "Recent work on mid-latitude and equatorial sporadic-E," *J. Atmos. Terr. Phys.*, vol. 51, no. 5, pp. 401–424, 1989, doi: 10.1016/0021-9169(89)90122-0. [Online]. Available: https://www.sciencedirect.com/science/article/pii/0021916989901220

[31] C. Haldoupis, D. Pancheva, W. Singer, C. Meek, and J. Macdougall, "An explanation for the seasonal dependence of midlatitude sporadic E layers," *J. Geophys. Res*, vol. 112, no. A6, 2007, doi: 10.1029/2007JA012322.

[32] J. Wright, L. R. Wescott, and D. J. Brown, "Mean electron density variations of the quiet ionosphere," US Dept. of Commerce, Office of Tech. Services, Washington, DC, USA, Jun. 1959. [Online]. Available: https://nvlpubs.nist.gov/nistpubs/Legacy/TN/nbstechnicalnote40-4.pdf

[33] B. W. Reinisch, X. Huang, I. A. Galkin, V. Paznukhov, and A. Kozlov, "Recent advances in real-time analysis of ionograms and ionospheric drift measurements with digisondes," *J. Atmos. Sol. Terr. Phys.*, vol. 67, no. 12, pp. 1054–1062, 2005, doi: 10.1016/j.jastp.2005.01.009. [Online]. Available: https://www.sciencedirect.com/science/article/pii/S1364682605000866

[34] I. A. Galkin and B. W. Reinisch, "The new artist 5 for all digisondes," Univ. of Massachusetts Lowell Center for Atmospheric Res., Lowell, MA, USA, 2008. [Online]. Available: https://www.ursi.org/files/CommissionWebsites/INAG/web-69/2008/artist5-inag.pdf

[35] M. Pezzopane and C. Scotto, "Software for the automatic scaling of critical frequency f0F2 and MUF(3000)F2 from ionograms applied at the Ionospheric Observatory of Gibilmanna," *Ann. Geophys.*, vol. 47, no. 6, 2004, pp. 1783–1790.

[36] M. Pezzopane and C. Scotto, "Highlighting the F2 trace on an ionogram to improve Autoscala performance," *Comput. Geosci.*, vol. 36, no. 9, pp. 1168–1177, 2010, doi: 10.1016/j.cageo.2010.01.010. [Online]. Available: https://www.sciencedirect.com/science/article/pii/S0098300410001652

[37] M. McDonnell, "Wavelet based detection and fitting of backscatter ionogram leading edges," 2014. [Online]. Available: https://www.researchgate.net/publication/242355969_WAVELET_BASED_DETECTION_AND_FITTING_OF_BACKSCATTER_IONOGRAM_LEADING_EDGES

[38] S. T. Hutchinson, "Scaling backscatter 1F leading edges," DST Group, Internal Rep., 1994.

[39] M. S. Penzin, S. N. Ponomarchuk, V. P. Grozov, and V. I. Kurkin, "Real-time techniques for interpretation of ionospheric backscatter sounding data," *Radio Sci.*, vol. 54, no. 5, pp. 480–491, 2019, doi: 10.1029/2018RS006656.

[40] H. Song, Y. Hu, C. Jiang, C. Zhou, and Z. Zhao, "Automatic scaling of HF swept-frequency backscatter ionograms," *Radio Sci.*, vol. 50, no. 5, pp. 381–392, 2015, doi: 10.1002/2014RS005621.

[41] J. Xue, C. Zhang, B. Yin, X. Jia, J. Xu, and M. Ma, "Ionogram echo extraction based on the convolutional neural networks," *Radio Sci.*, vol. 57, no. 6, 2022, Art. no. e2022RS007459. [Online]. Available: https://agupubs.onlinelibrary.wiley.com/doi/abs/10.1029/2022RS007459

[42] L.-C. Tsai and F. T. Berkey, "Ionogram analysis using fuzzy segmentation and connectedness techniques," *Radio Sci.*, vol. 35, no. 5, pp. 1173–1186, 2000. [Online]. Available: https://agupubs.onlinelibrary.wiley.com/doi/abs/10.1029/1999RS002170

[43] V. Pillat, L. Guimarães, P. Fagundes, and J. Silva, "A computational tool for ionosonde CADI's ionogram analysis," *Comput. Geosci.*, vol. 52, pp. 372–378, Mar. 2013, doi: 10.1016/j.cageo.2012.11.009.

[44] C. Jiang et al., "Improvement of automatic scaling of vertical incidence ionograms by simulated annealing," *J. Atmos. Sol. Terr. Phys.*, vol. 133, pp. 178–184, Oct. 2015, doi: 10.1016/j.jastp.2015.09.002. [Online]. Available: https://www.sciencedirect.com/science/article/pii/S1364682615300432

[45] C. Jiang et al., "Software for scaling and analysis of vertical incidence ionograms-ionoscaler," *Adv. Space Res.*, vol. 59, no. 4, pp. 968–979, 2017, doi: 10.1016/j.asr.2016.11.019.

[46] F. Su, Z. Zhao, S. Li, M. Yao, G. Chen, and Y. Zhou, "Signal identification and trace extraction for the vertical ionogram," *IEEE Geosci. Remote Sens. Lett.*, vol. 9, no. 6, pp. 1031–1035, Nov. 2012, doi: 10.1109/LGRS.2012.2189350.

[47] I. A. Galkin, B. W. Reinisch, G. A. Ososkov, E. G. Zaznobina, and S. P. Neshyba, "Feedback neural networks for ARTIST ionogram processing," *Radio Sci.*, vol. 31, no. 5, pp. 1119–1128, 1996. [Online]. Available: https://agupubs.onlinelibrary.wiley.com/doi/abs/10.1029/96RS01513

[48] V. Mochalov and A. Mochalova, "Extraction of ionosphere parameters in ionograms using deep learning," *E3S Web Conf.*, vol. 127, Nov. 2019, Art. no. 01004, doi: 10.1051/e3sconf/201912701004.

[49] C. De La Jara and C. Olivares, "Ionospheric echo detection in digital ionograms using convolutional neural networks," *Radio Sci.*, vol. 56, no. 8, 2021, Art. no. e2020RS007258. [Online]. Available: https://agupubs.onlinelibrary.wiley.com/doi/abs/10.1029/2020RS007258

[50] Y. Zheng, X. Wang, Y. Luo, H. Tian, and Z. Chen, "Segmentation and edge detection for ionogram automatic scaling," in *Proc. Int. Conf. Mach. Learn., Cloud Comput. Intell. Mining (MLCCIM)*, 2022, pp. 115–120, doi: 10.1109/MLCCIM55934.2022.00026.

[51] Z. Chen, S. Wang, S. Zhang, G. Fang, and J. Wang, "Automatic scaling of F layer from ionograms," *Radio Sci.*, vol. 48, no. 3, pp. 334–343, 2013, doi: 10.1002/rds.20038.

[52] Z. Chen, Z. Gong, F. Zhang, and G. Fang, "A new ionogram automatic scaling method," *Radio Sci.*, vol. 53, no. 9, pp. 1149–1164, 2018. [Online]. Available: https://agupubs.onlinelibrary.wiley.com/doi/abs/10.1029/2018RS006574

[53] Z. Ding, B. Ning, W. Wan, and L. Liu, "Automatic scaling of F2-layer parameters from ionograms based on the empirical orthogonal function (EOF) analysis of ionospheric electron density," *Earth Planets Space*, vol. 59, no. 1, pp. 51–58, 2007, doi: 10.1186/BF03352022.

[54] C. Jiang, G. Yang, Z. Zhao, Y. Zhang, P. Zhu, and H. Sun, "An automatic scaling technique for obtaining F2 parameters and F1 critical frequency from vertical incidence ionograms," *Radio Sci.*, vol. 48, no. 6, pp. 739–751, 2013. [Online]. Available: https://agupubs.onlinelibrary.wiley.com/doi/abs/10.1002/2013RS005223

[55] J. E. Titheridge, "A new method for the analysis of ionospheric h′(f) records," *J. Atmos. Terr. Phys.*, vol. 21, no. 1, pp. 1–12, 1961, doi: 10.1016/0021-9169(61)90185-4. [Online]. Available: https://www.sciencedirect.com/science/article/pii/0021916961901854

[56] J. E. Titheridge, "The overlapping-polynomial analysis of ionograms," *Radio Sci.*, vol. 2, no. 10, pp. 1169–1175, 1967, doi: 10.1002/rds19672101169.

[57] J. E. Titheridge, "Single-polynomial analysis of ionograms," *Radio Sci.*, vol. 4, no. 1, pp. 41–51, 1969, doi: 10.1029/RS004i001p00041.

[58] J. E. Titheridge, "The relative accuracy of ionogram analysis techniques," *Radio Sci.*, vol. 10, no. 6, pp. 589–599, 1975, doi: 10.1029/RS010i006p00589.

[59] M. W. Fox and C. Blundell, "Automatic scaling of digital ionograms," *Radio Sci.*, vol. 24, no. 6, pp. 747–761, 1989, doi: 10.1029/RS024i006p00747.

[60] N. Igi, K. Nozaki, M. Nagayama, A. Ohtani, H. Kato, and K. Igarashi, "Automatic ionogram processing systems in Japan," presented at the XXIVth General Assem. Int. Union Radio Sci. (URSI), Kyoto, Japan, Aug. 25–Sep. 2, 1993. [Online]. Available: https://www.ursi.org/files/CommissionWebsites/INAG/uag-104/text/igi.html

[61] D. R. Themens, B. Reid, and S. Elvidge, "ARTIST ionogram autoscaling confidence scores: Best practices," *URSI Radio Sci. Lett.*, vol. 4, pp. 1–5, Jan. 2022.

[62] M. Pezzopane and C. Scotto, "The INGV software for the automatic scaling of foF2 and MUF(3000)F2 from ionograms: A performance comparison with ARTIST 4.01 from Rome data," *J. Atmos. Sol. Terr. Phys.*, vol. 67, no. 12, pp. 1063–1073, 2005, doi: 10.1016/j.jastp.2005.02.022.

[63] M. Pezzopane and C. Scotto, "Automatic scaling of critical frequency foF2 and MUF(3000)F2: A comparison between Autoscala and ARTIST 4.5 on Rome data," *Radio Sci.*, vol. 42, no. 4, pp. 1–17, 2007, doi: 10.1029/2006RS003581.

[64] "Polan." GitHub. Accessed: Sep. 19, 2025. [Online]. Available: https://github.com/space-physics/POLAN

[65] J. E. Titheridge, "The real height analysis of ionograms: A generalized formulation," *Radio Sci.*, vol. 23, no. 5, pp. 831–849, 1988. [Online]. Available: https://agupubs.onlinelibrary.wiley.com/doi/10.1029/RS023i005p00831

[66] B. W. Reinisch, R. R. Gamache, H. Xueqin, and L. F. McNamara, "Real time electron density profiles from ionograms," *Adv. Space Res.*, vol. 8, no. 4, pp. 63–72, 1988, doi: 10.1016/0273-1177(88)90208-6. [Online]. Available: https://www.sciencedirect.com/science/article/pii/0273117788902086

[67] L. F. McNamara, "Quality figures and error bars for autoscaled Digisonde vertical incidence ionograms," *Radio Sci.*, vol. 41, no. 4, pp. 1–16, 2006, doi: 10.1029/2005RS003440.

[68] B. W. Reinisch et al., "New Digisonde for research and monitoring applications," *Radio Sci.*, vol. 44, no. 1, pp. 1–15, 2009, doi: 10.1029/2008RS004115.

[69] I. A. Galkin, B. W. Reinisch, X. Huang, and D. Bilitza, "Assimilation of GIRO data into a real-time IRI," *Radio Sci.*, vol. 47, no. 4, pp. 1–10, 2012, doi: 10.1029/2011RS004952.

[70] R. O. Conkright and L. F. McNamara, "Quality control of automatically scaled vertical incidence ionogram data," *Radio Sci.*, vol. 32, no. 5, pp. 1997–2002, 1997, doi: 10.1029/97RS01031.

[71] I. A. Galkin, B. W. Reinisch, X. Huang, and G. M. Khmyrov, "Confidence score of ARTIST-5 ionogram autoscaling," Lowell Digisonde Int., Lowell, MA, USA, INAG Tech. Memorandum, Nov. 2013. [Online]. Available: https://www.ursi.org/files/CommissionWebsites/INAG/web-73/confidence_score.pdf

[72] M. Pezzopane and C. Scotto, "A method for automatic scaling of F1 critical frequencies from ionograms," *Radio Sci.*, vol. 43, no. 2, pp. 1–12, 2008, doi: 10.1029/2007RS003723.

[73] C. Scotto and M. Pezzopane, "A method for automatic scaling of sporadic E layers from ionograms," *Radio Sci.*, vol. 42, no. 2, pp. 1–5, 2007, doi: 10.1029/2006RS003461.

[74] M. Pezzopane, C. Scotto, L. Tomasik, and I. Krasheninnikov, "Autoscala: An aid for different ionosondes," *Acta Geophys.*, vol. 58, no. 3, pp. 513–526, 2010, doi: 10.2478/s11600-009-0038-1.

[75] J. K. Ayliffe et al., "The DST group high-fidelity, multichannel oblique incidence ionosonde," *Radio Sci.*, vol. 54, no. 1, pp. 104–114, 2019, doi: 10.1029/2018RS006681.

[76] L. J. Nickisch, S. Fridman, M. Hausman, and G. S. San Antonio, "Feasibility study for reconstructing the spatial-temporal structure of TIDs from high-resolution backscatter ionograms," *Radio Sci.*, vol. 51, no. 5, pp. 443–453, 2016, doi: 10.1002/2015RS005906.

[77] P. L. Dyson, J. C. Devlin, R. Norman, and M. Parkinson, "The TIGER radar: An extension of SuperDARN to sub-auroral latitudes," in *Proc. Workshop Appl. Radio Sci.*, 2000, pp. 9–31.

[78] E. C. Bland, A. J. McDonald, S. de Larquier, and J. C. Devlin, "Determination of ionospheric parameters in real time using SuperDARN HF Radars," *J. Geophys. Res. Space Phys.*, vol. 119, no. 7, pp. 5830–5846, 2014, doi: 10.1002/2014JA020076.

[79] G. Chen, Z. Zhao, S. Li, and S. Shi, "WIOBSS: The Chinese low-power digital ionosonde for ionospheric backscattering detection," *Adv. Space Res.*, vol. 43, no. 9, pp. 1343–1348, 2009, doi: 10.1016/j.asr.2009.01.001. [Online]. Available: https://www.sciencedirect.com/science/article/pii/S0273117709000283

[80] T. A. Croft, "Sky-wave backscatter: A means for observing our environment at great distances," *Rev. Geophys.*, vol. 10, no. 1, pp. 73–155, 1972, doi: 10.1029/RG010i001p00073.

[81] C. Crouch, "Using neural networks and deep learning to improve ionospheric model accuracy using high-frequency radar backscatter observations," Masters Res. thesis, Univ. of Adelaide, Adelaide, South Australia, 2018.

[82] Y. LeCun, Y. Bengio, and G. Hinton, "Deep learning," *Nature*, vol. 521, no. 7553, pp. 436–444, 2015, doi: 10.1038/nature14539

[83] M. A. Cervera and T. J. Harris, "Modeling ionospheric disturbance features in quasi-vertically incident ionograms using 3-D magnetoionic ray tracing and atmospheric gravity waves," *J. Geophys. Res. Space Phys.*, vol. 119, no. 1, pp. 431–440, 2014, doi: 10.1002/2013JA019247.

[84] A. J. Heitmann et al., "Observations and modeling of traveling ionospheric disturbance signatures from an Australian network of oblique angle-of-arrival sounders," *Radio Sci.*, vol. 53, no. 9, pp. 1089–1107, 2018, doi: 10.1029/2018RS006613.

[85] L. H. Pederick, M. A. Cervera, and T. J. Harris, "Interpreting observations of large-scale traveling ionospheric disturbances by ionospheric sounders," *J. Geophys. Res. Space Phys.*, vol. 122, no. 12, pp. 12,556–12,569, Dec. 2017, doi: 10.1002/2017JA024337.

[86] M. Cordts et al., "The cityscapes dataset for semantic urban scene understanding," in *Proc. IEEE Conf. Comput. Vis. Pattern Recognit. (CVPR)*, 2016, pp. 3213–3223, doi: 10.1109/CVPR.2016.350.

[87] R. D. Hunsucker, "An atlas of oblique-incidence high-frequency backscatter ionograms of the midlatitude ionosphere," Inst. for Telecommun. Sci., Boulder, CO, USA, ESSA Tech. Rep. ERL; 162, pp. 105–108, 1970.

[88] I. A. Galkin, D. F. Kitrosser, Z. Kecic, and B. W. Reinisch, "Internet access to ionosondes," *J. Atmos. Sol. Terr. Phys.*, vol. 61, no. 1–2, pp. 181–186, 1999, doi: 10.1016/S1364-6826(98)00126-6.

[Online]. Available: https://www.sciencedirect.com/science/article/pii/S1364682698001266

[89] Z. Gong, P. Zhong, and W. Hu, "Diversity in machine learning," *IEEE Access*, vol. 7, pp. 64,323–64,350, 2019, doi: 10.1109/ACCESS.2019.2917620.

[90] S. Minaee, Y. Boykov, F. Porikli, A. Plaza, N. Kehtarnavaz, and D. Terzopoulos, "Image segmentation using deep learning: A survey," *IEEE Trans. Pattern Anal. Mach. Intell.*, vol. 44, no. 7, pp. 3523–3542, Jul. 2022, doi: 10.1109/TPAMI.2021.3059968.

[91] X. Li et al., "Transformer-based visual segmentation: A survey," 2023, *arXiv:2304.09854*.

[92] K. Banachewicz, L. Massaron, and A. Goldbloom, *The Kaggle Book: Data Analysis and Machine Learning for Competitive Data Science*. Birmingham, U.K.: Packt, 2022. [Online]. Available: https://books.google.com.au/books?id=GAVsEAAAQBAJ

GRS